Summer 8-2-2017

Viscoelastic Analysis and Fatigue Characterization of Bituminous Materials in Two Length Scales Under the Influence of Aging

Santosh Reddy Kommidi
University of Nebraska-Lincoln, santosh.kommidi@gmail.com

VISCOELASTIC ANALYSIS AND FATIGUE CHARACTERIZATION OF BITUMINOUS MATERIALS IN TWO LENGTH SCALES UNDER THE INFLUENCE OF AGING

By

Santosh Reddy Kommidi

A THESIS

Presented to the Faculty of

The Graduate College at the University of Nebraska

In Partial Fulfillment of Requirements

For the Degree of Master of Science

Major: Civil Engineering

Under the Supervision of Professor Yong-Rak Kim

Lincoln, Nebraska

July, 2017

VISCOELASTIC ANALYSIS AND FATIGUE CHARACTERIZATION IN TWO LENGTH SCALES UNDER THE INFLUENCE OF AGING

Santosh Reddy Kommidi, M.S

University of Nebraska, 2017

Advisor: Yong-Rak Kim

Fatigue cracking in asphalt concrete (AC) is of immense importance to pavement design and analysis because it is one of the most important forms of distress that can lead to structural failure in pavement. Once started, these types of cracks can be combined with other environmental factors leading to detrimental effects such as faster rates of pavement deterioration and shortened pavement life and functionality.

Currently AASHTO TP101, also known as linear amplitude sweep (LAS) specification, is being widely used to evaluate the ability of an asphalt binder to resist fatigue. The LAS method, although mechanistic in its approach, has certain drawbacks. First, the test is performed on an aged 2-mm thick binder sample, which in reality may never exist in the AC where there is a varying non-uniform thickness of the binder across the components of the AC. Secondly, the test methodology predicts an increased fatigue resistance at lower strain levels of load when the binder ages. This is in contrast to the general belief among researchers that aging is one of the primary contributors to the acceleration of pavement cracking.

This study aims to evaluate fatigue resistance in a more realistic approach that is more likely to exist in AC by incorporating sand asphalt mixtures. First, the linear viscoelastic properties of binder and sand asphalt mixture samples were evaluated to obtain the material properties under the influence of aging. Later, the fatigue tests on the sand asphalt mixture were investigated to understand the influence of a thin film of binder on the fatigue resistance. It was observed that G^R based energy dissipation

criterion for the binder evaluated a reasonable estimate for fatigue damage at relatively lower temperatures, but was limited to capture the influence of aging. Moreover, it was observed that fatigue testing on a binder at an intermediate temperature of 25 °C could cause edge effects to dominate as seen in the plateau regime for the phase angle in the time sweep tests. In order to overcome the edge effects in the binder LAS tests, the sand asphalt mixture testing was used for analyzing the binder fatigue resistance. Sand asphalt mixture testing could capture the microcracking and macrocracking phases more distinctively when compared to binder testing. In the case of pressure aging vessel (PAV) aged samples, it was observed that the macrocracking phase disappeared and was replaced by sudden changes in the material properties, indicating that the PAV aged mixture was more susceptible to fatigue cracking. By using the simplified viscoelastic continuum damage approach, the fatigue resistance of the binder and sand asphalt mixture was evaluated. The sand asphalt mixture testing was better to capture the influence of aging and changes in the microstructure during fatigue in comparison to binder fatigue tests.

DEDICATION

I dedicate this work to my parents!

ACKNOWLEDGEMENTS

First, I would like to thank Dr. Kim for giving me the opportunity to work with him. I thank him for the support, guidance, and discussions that have helped me move forward.

I would like to thank Dr. Jiong Hu and Dr. Mehrdad Negahban for being part of my thesis committee. I would like to thank them for their valuable input and suggestions that have helped me in completing my thesis.

I would like to thank my colleagues who have constantly helped and supported me ever since I have been at UNL.

TABLE OF CONTENTS

LIST OF FIGURES

LIST OF TABLES

CHAPTER ONE

INTRODUCTION

1.1 Overview

Fatigue cracking or failure is one of the most important forms of distress in asphalt pavements. There are four important forms of distresses: (1) fatigue cracking, (2) rutting or permanent deformation, (3) moisture induced damage, and (4) low temperature cracking. Most researchers are interested in these four forms of distress as they are critical to develop any predictive model of the pavement behavior over its life time, either computationally or analytically.

Fatigue cracking in asphalt pavement usually occurs due to repeated heavy axle loads from traffic. This could lead to development of various cracks in certain zones of the pavement across and along the wheel path. The exact location of these cracks on the pavement is quite difficult to predict as fatigue cracking in AC depends on various factors such as: (1) aggregate gradation, (2) air voids and their distribution, (3) binder properties, (4) variation of binder film thickness across the components of the AC, and (5) aging dependent changes in the properties of binder and AC [1]. The overall behavior and mechanical properties of the AC are highly dependent on the properties of the binder [2]. Also, there is a strong consensus among researchers that the weakest link in the composite mixture is the binder and the interface between the mastic and the aggregates. Fatigue cracks usually initiate and propagate in these two phases [3]. The significant impact of the binder properties on the fatigue resistance of AC is imperative, hence it is only natural that most studies to mitigate the fatigue cracking of AC are based on binder. Researchers have reported that based on the finite element simulation on AC, the stress and strain levels in the binder and mastic phase are at least 10 to 1000 more than what the pavement experiences [4-7]. This

occurs due to the differences in the stiffness of the aggregates, binder, and mastic phases.

There are several test methods and experimental procedures outlined in literature to investigate the fatigue resistance of the binder [8]. To analyze fatigue resistance characteristics one usually performs strain/stress sweep tests, time sweep tests at high levels of stress or strains, or more recently developed linear amplitude sweep (LAS) tests. Moreover, the binder properties are highly dependent on time, type of loading, temperature, and aging. It is important to incorporate these parameters or their effects in any mechanistic damage evolution analysis. To effectively characterize fatigue damage one must consider the following factors:

1. They must be more realistic in the sense that it should represent what truly happens in the pavement.
2. Well-defined damage evolution law
3. Well-defined failure criterion
4. The described method should be independent of path and type of loading.
5. The evolution of aging

In order to incorporate the effect of binder film thickness as observed in the pavement, fatigue tests on sand asphalt were investigated. Although sand asphalt is not a true representation of the state of the binder in the pavement, it does provide valuable insight in to the influence of thin films on fatigue resistance.

1.2 Objective and Scope

In the current investigation, the linear viscoelastic properties of bituminous materials in two different length scales, binder and sand asphalt, were obtained under the influence of aging.

The fatigue resistance was characterized in the two length scales using time sweep and stress/strain sweep tests under different loading conditions and temperatures. The results were then analyzed using the simplified viscoelastic continuum damage model, and the influence of aging on the fatigue life of the samples was assessed. The most recently developed average released pseudo strain energy method was used for binder, and its applicability for sand asphalt was assessed.

CHAPTER TWO

LITERATURE REVIEW

2.1 Introduction

Asphalt layer in pavements strongly behaves as viscoelastic, and it owes its nature to the properties of the binder used. Fatigue failure is the most commonly observed distress phenomenon in the asphalt pavements. This form of cracking usually appears along the wheel path of the pavement and is mostly due to the repeated heavy axle loads. Fatigue failure is closely associated with the mechanical properties of the asphalt binder used in the composite. Even though the binder used strongly influences the fatigue resistance of AC, there are other factors such as: (1) aggregate gradation, (2) air voids and their distribution, (3) binder properties, (4) variation of binder film thickness across the components of the AC, and (5) aging dependent changes in the properties of the binder that can influence the fatigue behavior in the AC. It is beyond the scope of the current investigation to consider all the factors. Instead, some of the factors such as aging, binder in the form of thin films, and small air voids will be investigated.

The most frequently used performance based specification for binder to mitigate the fatigue failure in AC is the PG grading system. It requires the binder to be tested under oscillatory mode at different aging conditions such as unaged, short term, and long term aged to evaluate the performance of the binders at intermediate and high temperatures to check the binder's ability to resist rutting and fatigue cracking. The parameter $|G^*| \sin(\delta)$ was used as to evaluate the fatigue resistance and limited it to a value of 5000 kPa. Several researchers such as Stuart and Mogawer and Tsai and Monismith [9] concluded that the $|G^*| \sin(\delta)$ parameter was a poor choice of material resistance to fatigue because of poor correlation compared to field fatigue

evaluation. Bahia et.al [10] suggested that the strain level used for the PG grading was relatively less compared to the actual strains experienced by the binder in the asphalt mixture composite. Hence, they suggested the fatigue testing methodology to incorporate high non-linear strain levels. In another study, Masad et.al [4] conducted finite element analysis on the microstructure of AC to investigate the influence of localized strain distribution on the mechanical response of the composite. It was concluded that the strain levels in the mastic or the binder phase were quite high and most likely to be in the non-linear region. In order to incorporate the effects of high strain levels, Bahia et al. [11] suggested the use of time sweep tests to evaluate cracking in the asphalt binder. Anderson et al. [12] thoroughly investigated the time sweep tests proposed by Bahia et al. [11] and suggested that when the binder modulus was low at the intermediate temperatures, the binder was susceptible to edge effects and instability flow, and such fatigue characterization would not represent true fatigue behavior. They suggested that fatigue characterization should be performed at relatively low temperatures where the binder stiffness would be large enough to avoid edge effects. Kim et al. [13] were the first to introduce the testing of a thin film of binder by incorporating fatigue tests on sand asphalt mixtures. They proposed a new sample fabrication methodology where uniformly graded Ottawa sand particles were mixed with 8% of the weight of the binder. The samples were 50 mm in height and 12 mm in diameter, and time sweep tests were performed on these cylindrical samples using a dynamic mechanical analyzer. The proposed method ensured that there were no edge effects as the sample was much stiffer and could represent the true state of binder in the AC mixture. Their methodology was based on a mechanistic approach incorporated a viscoelastic continuum damage-based analysis. They identified that the second point of inflection in the stiffness versus the number of cycles and the peak in

phase angles correlated well to describe the point of fatigue failure in the samples. They also investigated the influence of rest periods on the fatigue life of sand asphalt samples. In another study, Martono et al. [14] investigated the influence of edge flow and instability parallel to the plate testing of the binder by comparing time sweep results of the binder and sand asphalt samples. Simple shift parameters were used to compare the results from the two length scales, and regression analysis indicated that test geometry was not a sufficiently significant factor to affect the fatigue results in the binder, and that there were no significant edge effects.

Over the last two decades there has been significant improvement in characterizing fatigue damage in asphalt concrete based on the continuum damage models. Continuum damage theory is developed based on the changes observed in material properties at the macroscale (15). One of the most frequently used approaches in characterizing fatigue damage in AC is the viscoelastic continuum damage (VECD) theory based on the crack growth in viscoelastic media by Schapery [16]. A similar approach was used here for binder and sand asphalt mixture samples to assess the fatigue resistance properties.

CHAPTER THREE

EXPERIMENTAL PROCEDURE

3.1 Experimental Outline

The mechanical properties of bituminous materials are highly dependent on time, temperature, and type of load applied. Any testing methodology adopted should be able to capture such dependencies to better understand the material response and model the material properties appropriately. Throughout the investigation, the load applied to the sample was either in controlled strain mode or stress mode, and all tests on both the binder and sand asphalt mixture were performed in torsion. Typically, bituminous materials are subjected to two types of testing, either in the time domain or in the frequency domain. Since the material dependent properties are the same irrespective of the type of domain used, one can convert material properties in one domain to another. Another mode of testing that is quite frequently used is the oscillatory mode of testing where the sample is subjected to a sinusoidal loading. The response measured would also be a sinusoidal response but out of phase relative to the applied load.

3.2 Materials

The binder selected for all the tests performed in this thesis is PG 64-28. It is the most commonly used binder in the state of Nebraska apart from PG 64-34 and PG 58-34. The PG 64-34 and PG 64-28 are polymer modified binders whereas the PG 58-34 is an unmodified binder.

For preparing sand asphalt mixture samples, Ottawa sand was used with binder at a dosage of 4% by the weight of the binder. The selected Ottawa sand met the specification of ASTM C778 graded sand. The reason for using the sand asphalt

mixture for this study is to assess the influence of a thin film of binder on the fatigue resistance and the overall mechanical properties of the sand-binder composite.

3.3 Sample Preparation

3.3.1 Binder

As mentioned above, the binder used in this investigation is a PG 64-28 polymer modified binder. Typically, the PG 54-49 base binder from the source was modified with a dosage of 4% of Styrene butadiene styrene polymer and blended using a high shear mixer to obtain the PG 64-28 binder.

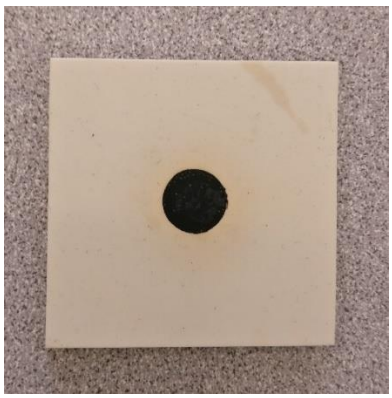

Figure 3.1 Hot binder poured into an 8mm diameter silicone mold and allowed to cool

3.3.2 Sand Asphalt

The sand asphalt samples were prepared in two stages. In the first stage, called the mixing stage, the sand particles and binder were thoroughly mixed at an elevated temperature and stored in small containers. Then in a later stage called the compaction stage, the mixture was compacted to cylindrical samples in a metallic mold. In the mixing stage about 700 g of Ottawa sand was heated to a temperature of 135 °C for 30 min in an oven then the binder, which was also heated to the same temperature,

was poured into the mixture and allowed to heat for 15 minutes. Once out of the oven, the mixture was mixed thoroughly until all the sand particles were coated with binder. If necessary (in case of short term aged samples), the mix was placed in the oven for another 15 minutes and mixed again until all the particles were coated with a thin film of binder. The mixture was stored in small containers and stored at a low temperature until it was used for compacting. In the compaction stage, approximately 10.5 g of a sand asphalt mixture in a small container was placed in the oven at 100 °C. After 20 minutes, the mixture was poured into the mold immediately and compacted manually to obtain cylindrical samples with a height of 50 mm and a diameter of 12.3 mm. The same weight of the sand asphalt mixture was used for compaction to maintain consistency across the samples prepared. The mold was allowed to cool down so that the cylindrical samples would easily be removed from the mold. The samples were later glued to clamps using an epoxy based glue.

3.4 Experimental Tests

3.4.1 Strain/Stress Sweep

In order to identify linear viscoelastic regime, a strain (or stress) sweep experiment can be conducted. In the strain (or stress) sweep experiment, the samples are subjected to increasing strain (or stress) levels with time, and the changes in the complex modulus value are observed. If the material was to satisfy the homogeneity condition of linear viscoelasticity, then the $|G^*|$ values will not change with varying strains (or stresses). If the $|G^*|$ values begin to drop, then the stress (or stress) levels are no longer in the linear regime, and the material behaves non-linearly.

3.4.2 Frequency Sweep

Once the linear viscoelastic limits have been established using the strain (or stress) sweep experiments, frequency sweep tests are performed at various

temperatures to establish the materials' linear viscoelastic properties over a wide range of loading conditions. At a given temperature and strain selected, the frequency sweep test varies loading frequencies from 0.1 Hz to 10 Hz, and the values of |G*| and phase angle (δ) are obtained. A similar test is performed at various temperatures. A typical example for frequency sweep results on the binder and sand asphalt are shown in Figure 3.2 and Figure 3.4, respectively.

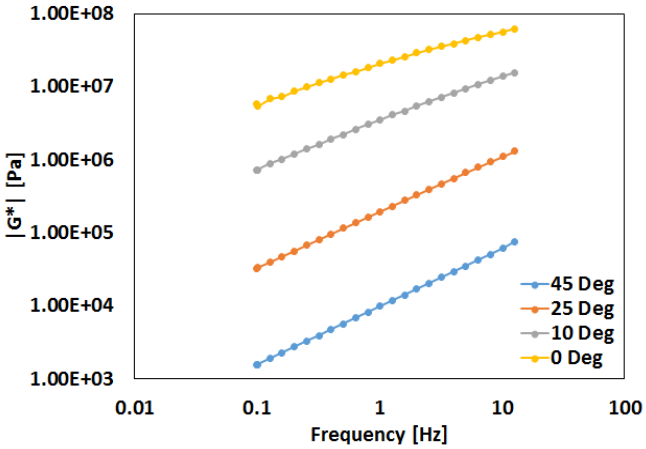

(a)

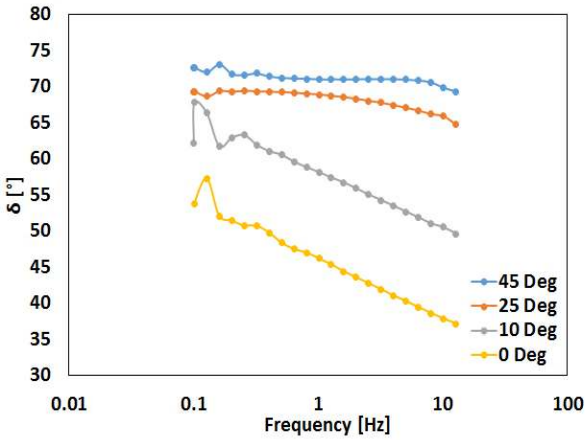

(b)

Figure 3.2 Frequency sweep data for unaged binder (a) |G*| vs frequency (b) δ vs frequency

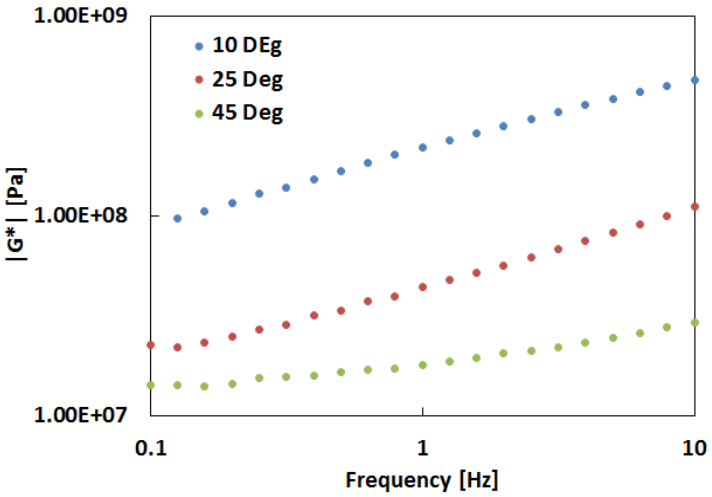

(a)

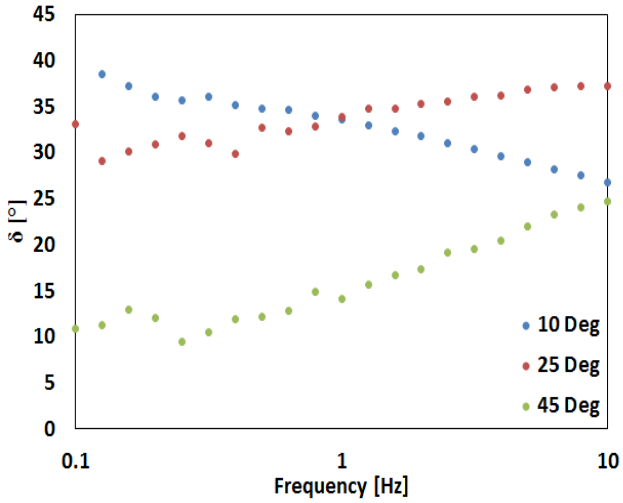

(b)

Figure 3.3 Frequency sweep data for unaged sand asphalt sample (a) |G*| vs frequency (b) δ vs frequency

3.4.3 Time Sweep

Fatigue damage in asphalt binder and sand asphalt is of primary concern in this study. To perform fatigue related tests, a time sweep test was done on binder and sand asphalt samples. In this test, the samples are subjected to a constant high non-linear peak strain (or stress) in the oscillatory mode at a frequency-temperature. As

the loading cycles increase, there is a drop in |G*| values, which can be associated with damage accumulation. The trend in the |G*| and δ values can tell how the material resists fatigue damage accumulation and when the samples failed. An example for the time sweep test done using the controlled strain mode on binder and sand asphalt are shown in Figure 3.4 and Figure 3.5, respectively, where N_f represents the number of cycles to failure. Later in chapter 5, the definition of failure and how to calculate the number of cycles to failure will be discussed in detail. The figures here only represent the trends one will notice in different samples tested and the type of loading mode used. For controlled stress time sweep results, the data for the unaged binder performed at a peak stress amplitude of 50 KPa is shown in Figure 3.6.

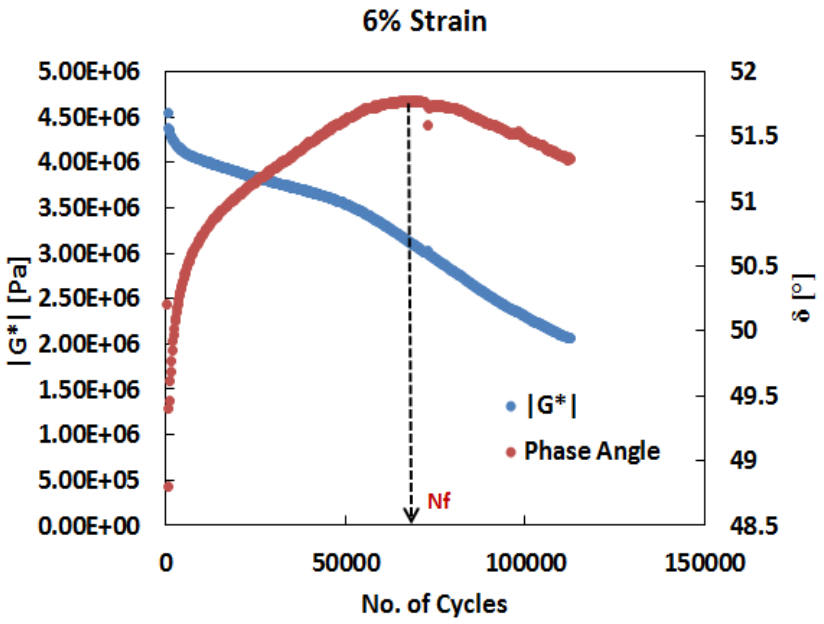

Figure 3.4 Time sweep |G*| and δ values for PAV age binder at 6 % strain amplitude.

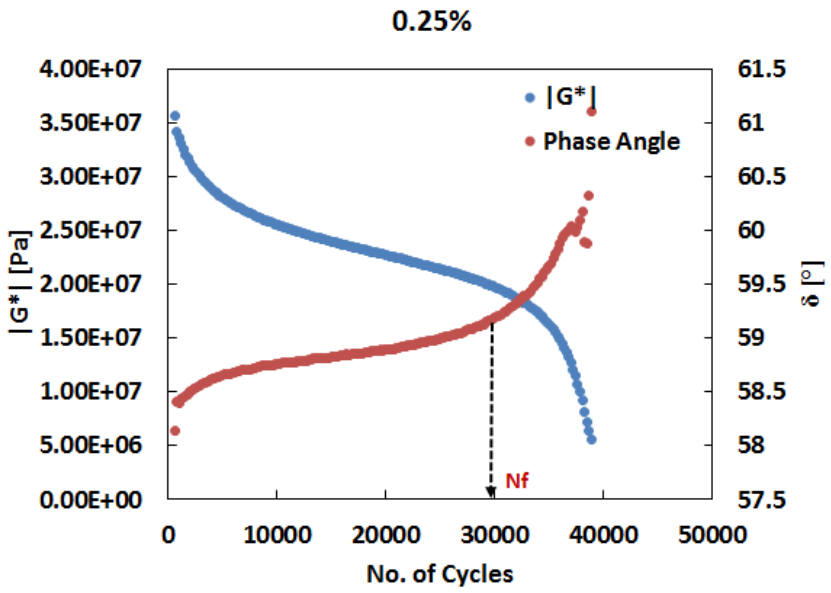

Figure 3.5 Time sweep |G*| and δ values for unaged sand asphalt sample at 0.25 % strain amplitude.

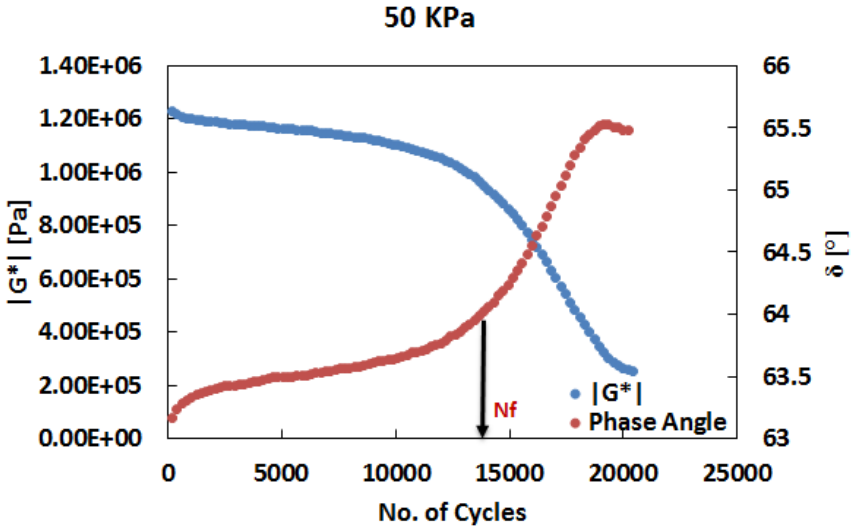

Figure 3.6 Time sweep |G*| and δ values for unaged binder at 50 KPa stress amplitude.

3.5 Equipment

To perform the time and frequency domain tests on binder and sand asphalt, two different shear rheometers were used. For all the tests performed on binder except

the time sweep tests, the Malvern DSR was used. For sand asphalt, AR 2000 Ex was used. Figure 3.7 and Figure 3.8 show the schematic representation of the two-equipment used in this study.

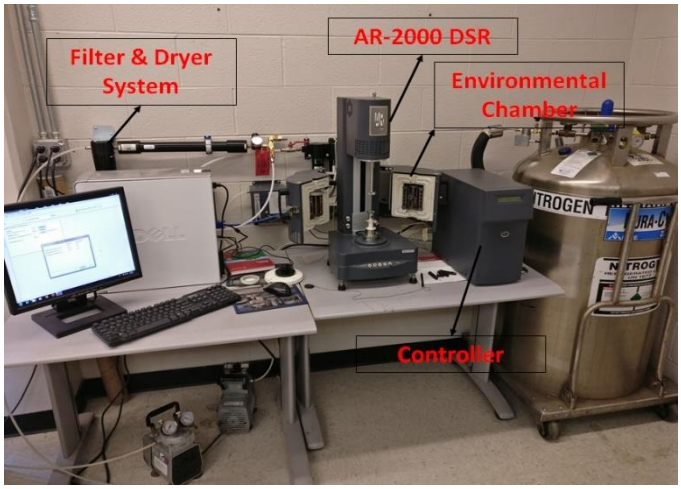

Figure 3.7 AR 2000 DSR and its components used for testing sand asphalt samples

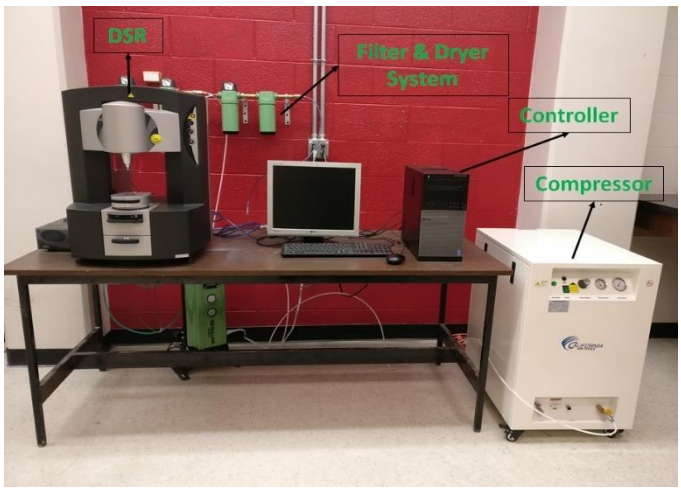

Figure 3.8 Malvern DSR and its components used for binder testing

Tests on binder were performed using a parallel plate geometry where the bottom plate was fixed and the top plate was free to rotate. The plate diameter used was 8 mm. The binder sample was placed in between the two plates, and the thickness

of the sample was set as 2 mm. Figure 3.9 shows the sample that was placed between the two plates.

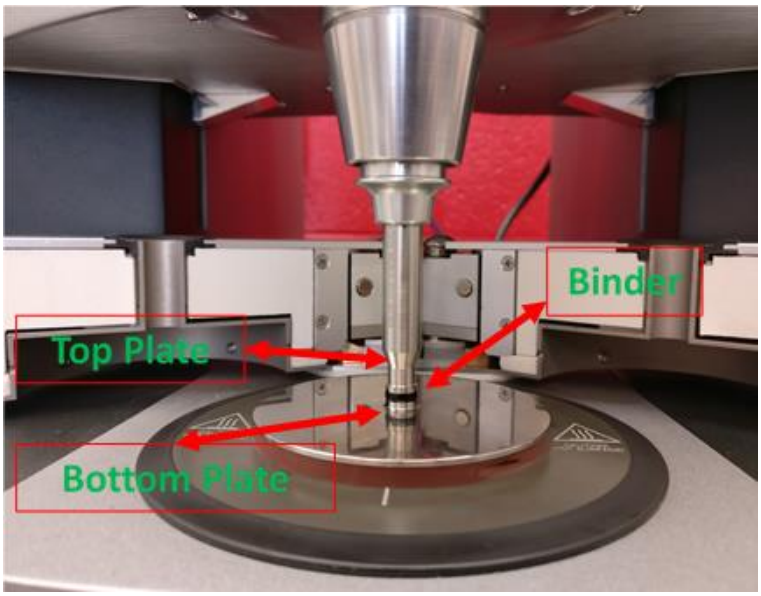

Figure 3.9 Binder placed between the top and bottom 8mm plate in Malvern DSR

CHAPTER FOUR

LINEAR VISCOELASTIC ANALYSIS OF BINDER AND SAND ASPHALT

4.1 Introduction to Linearity

A material is said to behave as a linear viscoelastic material if and only if it satisfies the following two important criteria: (1) homogeneity and (2) superposition. The above statement can be mathematically described in the two equations (Equations (4.1) and (4.2)) below [17]. This is the basis for the Bolzmann superposition principle.

$$R\{\alpha I\} = \alpha R\{I\} \tag{4.1}$$

$$R\{I_1 + I_2 + \cdots \ldots . + I_n\} = R\{I_1\} + R\{I_2\} + \cdots \ldots \ldots . . + R\{I_n\} \tag{4.2}$$

For a linear non-aging, isothermal viscoelastic material, stress-strain constitutive equation in shear can be represented by a Boltzmann superposition integral or also called as the convolution integral, as shown in Equations (4.3) and (4.4). $G(t)$ is called the shear relaxation modulus, $J(t)$ is called the shear creep compliance, and τ is the integration variable.

$$\sigma(t) = \int_0^t G(t-\tau)\frac{d\varepsilon\,(\tau)}{d\tau} \tag{4.3}$$

$$\varepsilon(t) = \int_0^t J(t-\tau)\frac{d\sigma\,(\tau)}{d\tau} \tag{4.4}$$

The above equations represent the time domain constitutive equations when input is controlled strain and stress, respectively. The form shown above is the integral representation of the constitutive equation, and it can also be represented in

its differential form. Such a response can be modeled using a combination of linear springs and dashpots, either in series or parallel, or a combination of both. Such representation helps in defining a mathematical form for $G(t)$ and $J(t)$ functions, as shown in Equations (4.5) and (4.6). G_∞, G_i and ρ_i are long time equilibrium modulus, relaxation modulus constants, and relaxation times, respectively. Similarly, $J_g,\ \eta_0,\ J_j$ and τ_j are glassy compliance, zero shear or long time viscosity, creep compliance constants and retardation times, respectively.

$$G(t) = G_\infty + \sum_{i=1}^{m} E_i\, e^{-\left(\frac{t}{\rho_i}\right)} \tag{4.5}$$

$$J(t) = J_g + \frac{t}{\eta_0} + \sum_{j=1}^{n} J_j \left(1 - e^{-\left(\frac{t}{\tau_j}\right)}\right) \tag{4.6}$$

The above form is known as the Prony series representation of a linear viscoelastic material. The material dependent functions such as $G(t)$ and $J(t)$ are interrelated, and one form can be converted to the other. The methods for converting one form to another is discussed in detail by Schapery (18).

In the frequency domain, complex material functions arise in response to the sinusoidal loading using the constitutive equations shown in Equations (4.3) and (4.4), where real parts are denoted by single prime, and the imaginary part by double primes (18). The real and imaginary parts are the storage and loss functions, respectively.

$$G^* = G'(\omega) + i\, G''(\omega) \tag{4.7}$$

$$J^* = J'(\omega) - i\, J''(\omega) \tag{4.8}$$

$$G'(\omega) = G_\infty + \sum_{i=1}^{m} \frac{\omega^2 \rho_i^2 G_i}{\omega^2 \rho_i^2 + 1} \tag{4.9}$$

$$G''(\omega) = \sum_{i=1}^{m} \frac{\omega \rho_i G_i}{\omega^2 \rho_i^2 + 1} \tag{4.10}$$

$$J'(\omega) = J_g + \sum_{i=1}^{n} \frac{J_i}{\omega^2 \tau_i^2 + 1} \tag{4.11}$$

$$J'(\omega) = \frac{1}{\eta_0 \omega} + \sum_{i=1}^{n} \frac{\omega_i \tau_i J_i}{\omega^2 \tau_i^2 + 1} \tag{4.12}$$

The method used to convert one form to another in the time and frequency domain and estimation of the constants are detailed by Park and Schapery [18]. A similar approach is utilized in the current investigation for estimating the Prony series representation of the shear modulus and creep compliance for binder and sand asphalt mixture. To that end, the first set of experiments that are performed on the binder and sand asphalt are to establish the linear viscoelastic regime. To obtain the linear regime, experiments based on time or frequency domain can be performed. In the present investigation, a series of strain sweep tests are conducted at different temperatures and frequencies for the binder and sand asphalt mixture samples, as shown in Table 4.1 and Table 4.2.

In Figure 4.1 it can be observed when the binder is well within the linear regime, the |G*| values are inderpendent of strains. A similar observation can be made for the phase angle, as shown in Figure 4.2.

Table 4.1 Binder test matrix

Test Type	Temperature	Frequency	Unaged	RTFOT	PAV
Strain Sweep	0 Deg	0.1 Hz	✓	✓	✓
		10 Hz	✓	✓	✓
	45 Deg	0.1 Hz	✓	✓	✓
		10 Hz	✓	✓	✓
Frequency Sweep	0 Deg	0.1 - 10 Hz	✓	✓	✓
	15 Deg		✓	✓	✓
	25 Deg		✓	✓	✓
	45 Deg		✓	✓	✓
	65 Deg		✓	✓	✓

Table 4.2 Sand asphalt test matrix

Test Type	Temperature	Frequency	Unaged	RTFOT	PAV
Strain Sweep	0 Deg	0.1 Hz	✓	✓	✓
		10 Hz	✓	✓	✓
	45 Deg	0.1 Hz	✓	✓	✓
		10 Hz	✓	✓	✓
Frequency Sweep	10 Deg	0.1- 10 Hz	✓	✓	✓
	25 Deg		✓	✓	✓
	45 Deg		✓	✓	✓

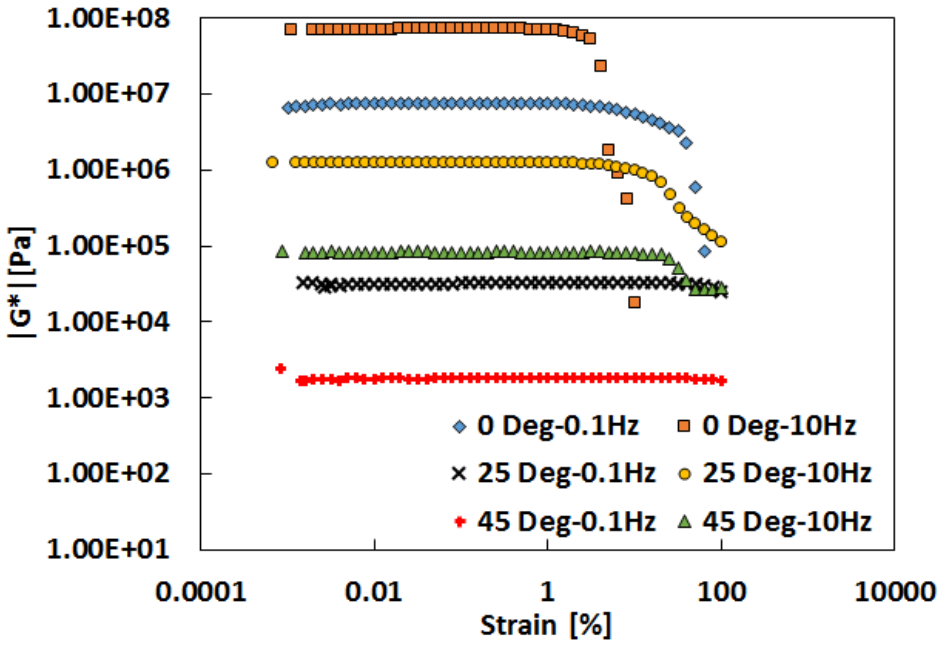

Figure 4.1 |G*| vs strain in a strain sweep tesst at different frequencies and temperatures for unaged binder

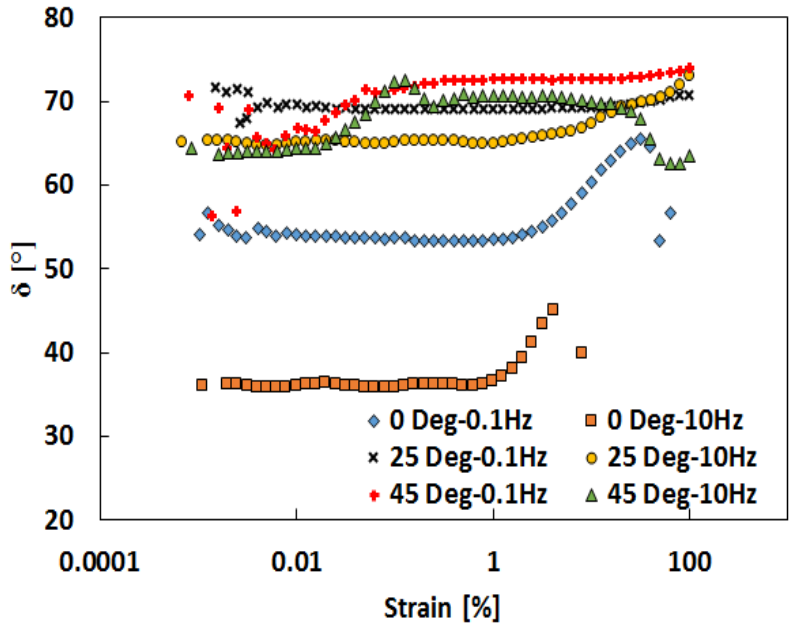

Figure 4.2 δ vs strain at different frequencies and temperatures for unaged binder

A similar trend as seen in |G*| and phase angle (δ) values in strain sweep tests on an unaged binder was observed in the RTFOT and PAV aged binder. It is to be noted that the low temperature (0 °C) and high frequency (10 Hz) plays a critical role in the binder linear behavior as it shifts the limits to lower strain values. Figure 4.3 shows the |G*| and phase angle (δ) values for the strain sweep test performed at a low temperature and high frequency for different aging conditions. Another point to be noted here is that the |G*| and phase angle independence can only justify the homogeneity requirement for linearity. Hence, even though the graphs suggest that linearity could be up to 1% strain, a lower strain value of 0.1% was taken to ensure that any subsequent tests are within the material's linear limits. Similar tests were performed on unaged, RTFOT, and PAV aged sand asphalt mixture samples. Example strain sweep test results from an unaged sand asphalt mixture are shown in Figure 4.4 and Figure 4.5.

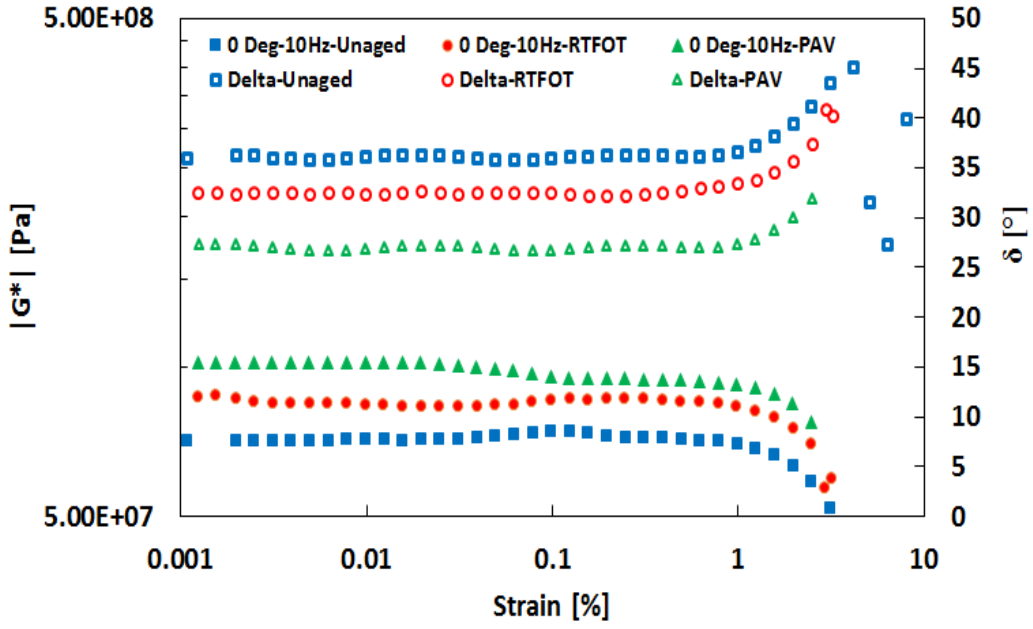

Figure 4.3 Strain sweep data at 0 °C and 10 Hz for unaged, RTFOt and PAV aged binders

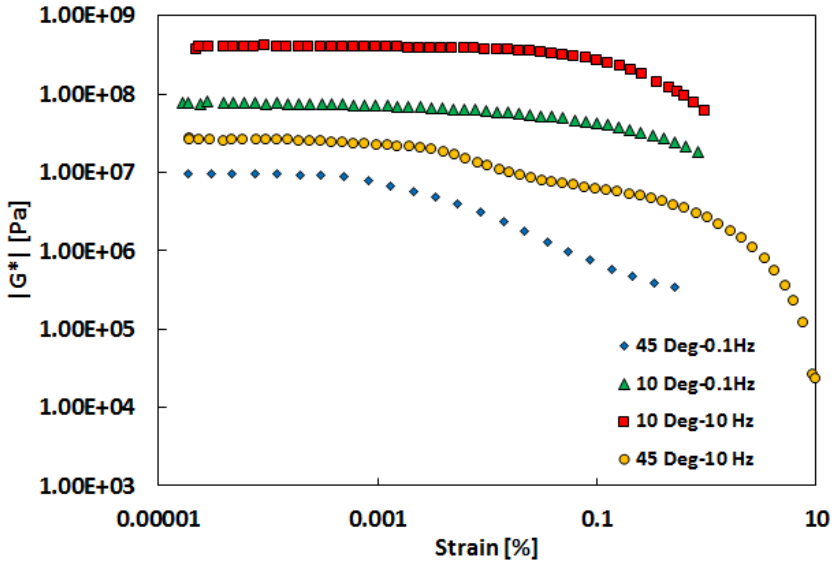

Figure 4.4 |G*| vs strain in strain sweep tests performed at different temperatures and frequencies for unaged sand asphalt mixture sample

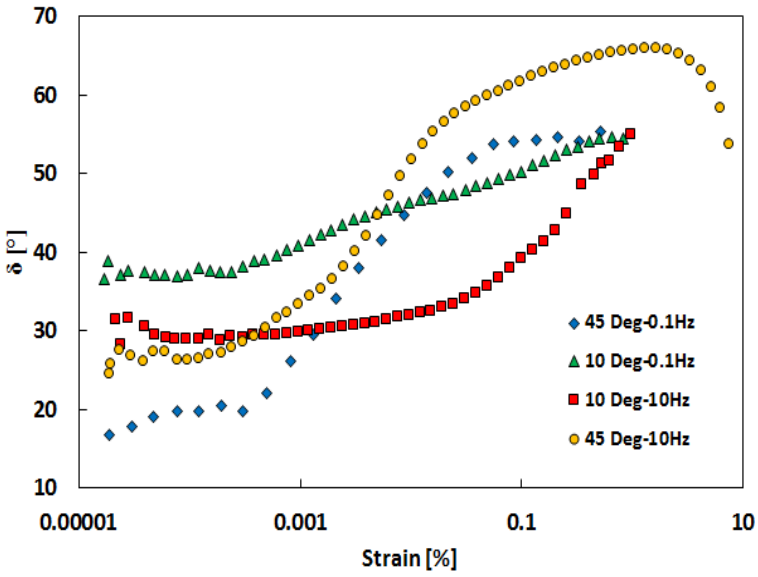

Figure 4.5 Phase angle (δ) vs strain in strain sweep tests performed at different temperatures and frequencies for unaged sand asphalt mixture sample

It can be observed in Figure 4.4 and Figure 4.5 that the trend in |G*| and phase angle values for an unaged sand asphalt mixture are different when compared to the

trends in an unaged binder. It clearly indicates the strong influence of the thin film of the binder on the overall properties of the mixture. In Figure 4.4 the linear limits are influenced by high temperature (45 °C) and low frequency (0.1 Hz), unlike the observations made in the unaged binder. Moreover, at these temperatures, the phase angle is lower than that of 10 °C, indicating that there are significant contacts occurring between the sand particles in the mixture. It can be concluded that the sand asphalt mixture is susceptible to large deformation, early and faster rates of damage at high temperatures where the binder film thickness controls the overall behavior of the mixture. Figure 4.6 and Figure 4.7 show the influence of aging on the strain sweep results.

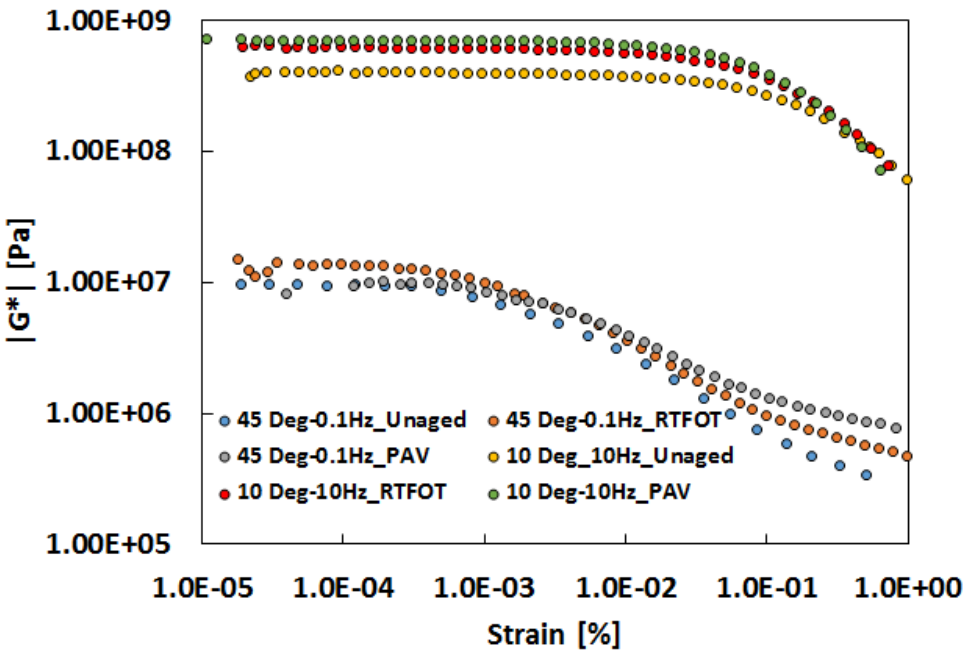

Figure 4.6 |G*| vs strain in strain sweep tests performed at different temperatures and frequencies for unaged, RTFOT, and PAV aged sand asphalt mxture sample

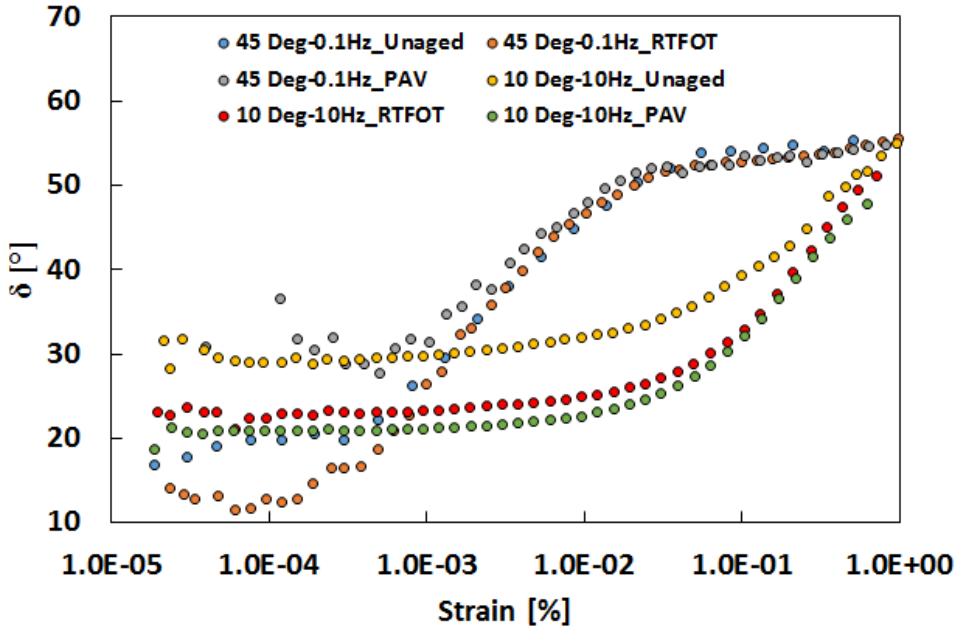

Figure 4.7 Phase angle (δ) vs strain in strain sweep tests performed at different temperatures and frequencies for unaged, RTFOT, and PAV aged sand asphalt mixture samples

4.2 Time-Temperature Superposition and Master Curve

Based on the strain sweep tests performed on binder and sand asphalt mixture samples, appropriate strain amplitudes were selected to perform frequency and temperature dependent tests to obtain the linear viscoelastic material properties. The strain amplitudes selected are shown in Table 4.3. Frequency sweep tests were performed over a wide range of temperature, as an example test on an RTFOT aged binder is shown in Figure 4.8 and Figure 4.9. The reason for performing tests at different temperatures is to use the principle of time-teperature superposition (TTSP), which says that the effect of time and temperature is equivalent for a linear viscoelatic material.

Table 4.3 Strain amplitude selected for performing frequency sweep tests

Aging	Binder	Sand Asphalt Mixture
Unaged	0.10%	$10^{-4}\%$
RTFOT aged	0.10%	$10^{-4}\%$
PAV aged	0.01%	$10^{-4}\%$

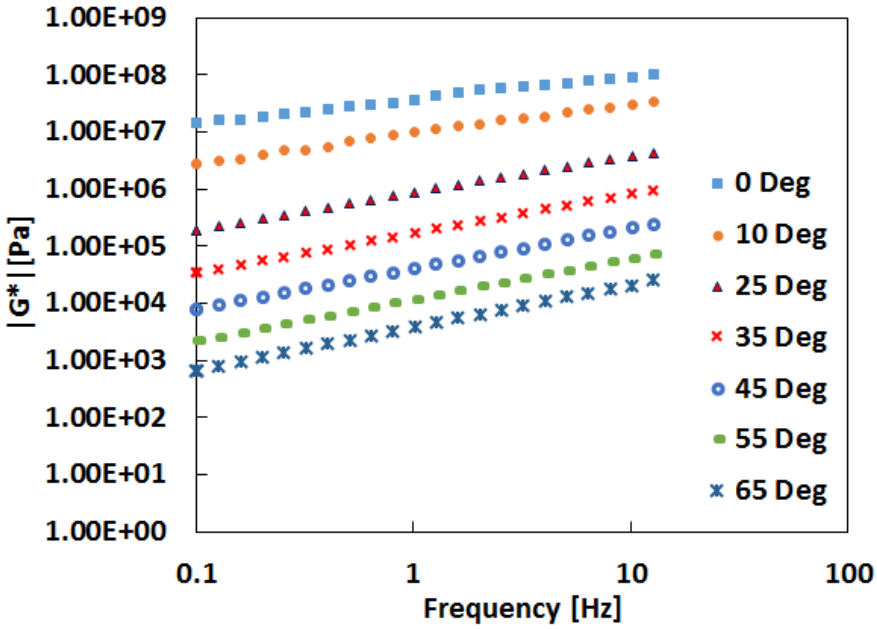

Figure 4.8 |G*| vs frequency in a frequeny sweep test performed at different temperatures on RTFOT aged binder

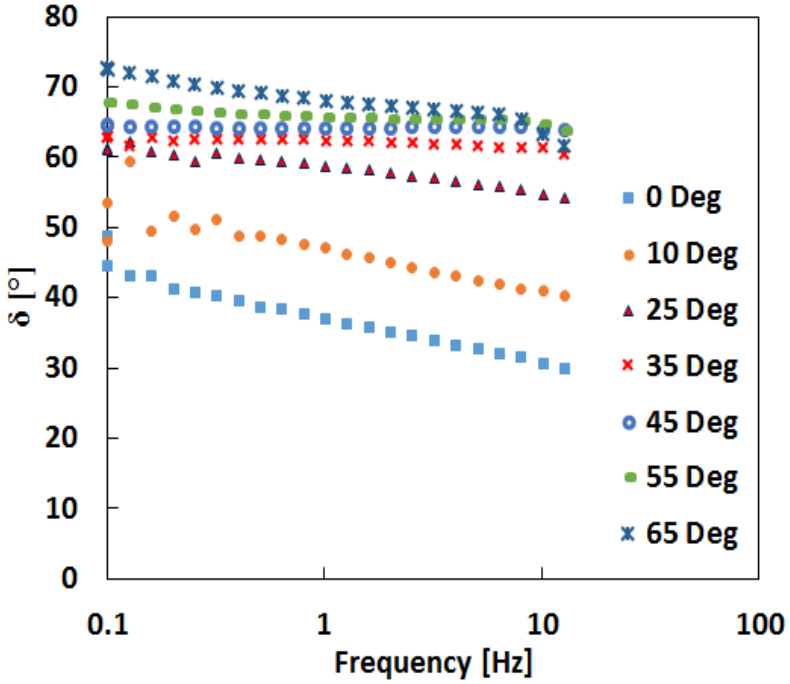

Figure 4.9 δ vs frequency in a frequeny sweep test performed at different temperatures on RTFOT aged binder

TTSP allows for the use of temperature dependent shift factors $(a_T(T))$ to move the curves at different temperatures in order to allign to a reference temperature curve. Using TTSP, as shown below in Equation (4.13), where ω_R is the reduced frequency, T_{ref} is the reference temperature and $a_T(T)$is the temperature dependent shift factor, one can shift to a reference temperature. Figure 4.10 shows the shifted curves using shift factors onto a reference temperature of 25 °C for an RTFOT aged binder. The resulting curve is called the master curve, which is representative of the material properties over a wide rage of loading frequency.

$$\omega_R(T_{ref}) = a_T(T) * \omega(T) \tag{4.13}$$

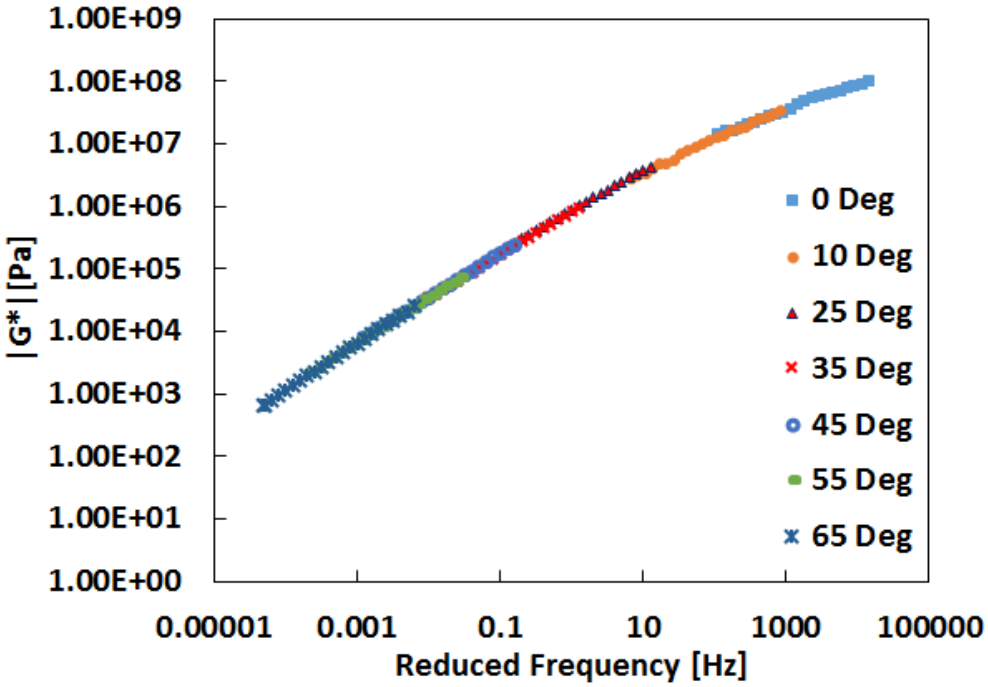

Figure 4.10 Shifted |G*| data for RTFOT aged binder

Figure 4.11 shows the master curve obtained for storage and loss modulus and phase angle using the same shift factor that was used for shear modulus for the RTFOT aged binder sample. It should be noted that, for TTSP to work for the binder or sand asphalt mixture, the same shift factors are applicable to loss modulus, storage modulus, and phase angle. Similarly, master curves were obtained for sand asphalt mixture samples under different aging conditions using TTSP. The shift factors identified for binders and sand asphalt mixtures are presented in Table 4.4 and Table 4.5 respectively.

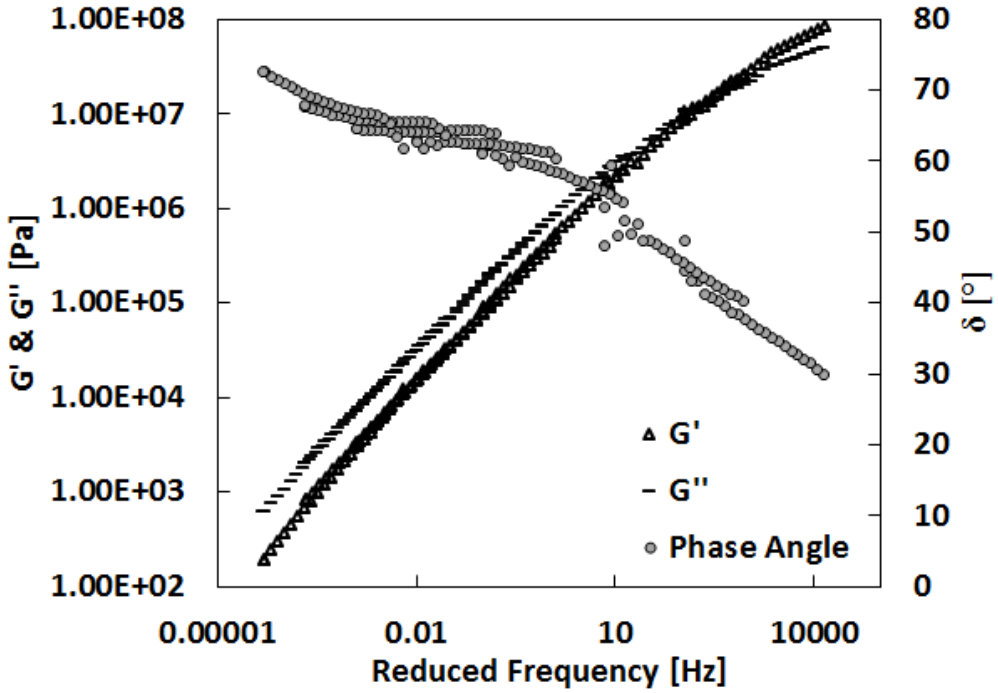

Figure 4.11 Shifted G', G'' and δ for RTFOT aged binder using the same shift factors

Table 4.4 Shift factors for binder

Temperature	a_T		
[° C]	Unaged	RTFOT	PAV
65	0.00095	0.0005	0.00035
55	-	0.0021	-
45	0.0185	0.0126	0.01
35	0.125	0.1	-
25	1	1	1
10	57	67	78
0	1129	1120	2480

Table 4.5 Shift factors for sand asphalt mixture

Temperature	a_T		
[° C]	Unaged	RTFOT	PAV
45	0.0355	0.023	0.02
25	1	1	1
10	55	73	89

Figure 4.12 shows the master curves obtained for binder and sand asphalt mixture samples under different aging conditions using TTSP, which works well for both materials when tested in the linear viscoelastic regime. There is a clear indication of the difference in the material properties in the two different length scales, and the influence of aging is clearly visible.

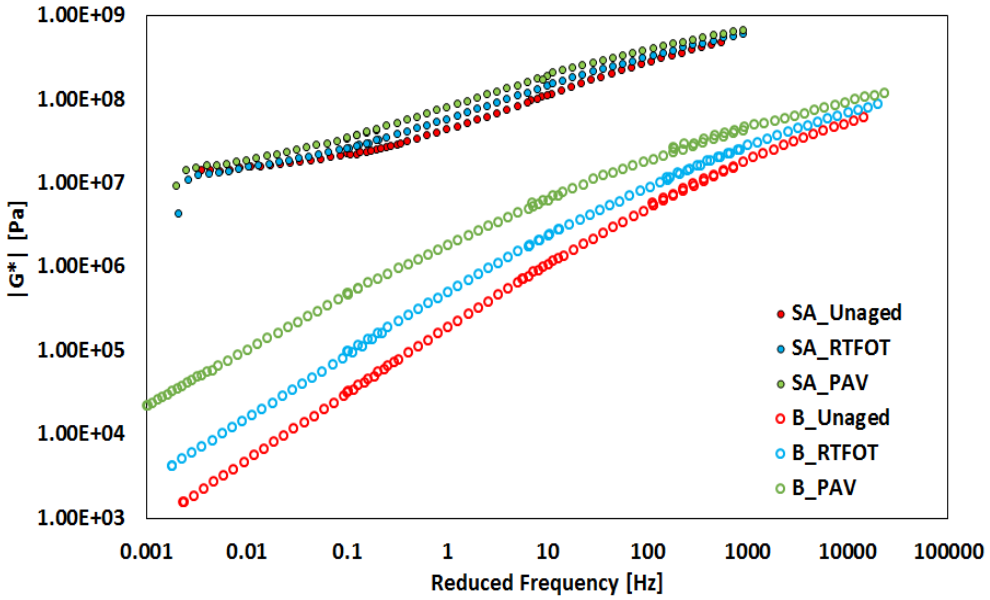

Figure 4.12 Master curve of binder and sand asphalt mixture samples for unaged, RTFOT, and PAV aged samples

The shear modulus values of the sand asphalt mixture is at least three orders of magnitude higher than the corresponding binder length scale. This is due to the fact that most of the sand asphalt mixture is composed of sand particles which are the main contributors to the sample stiffness. The change in slope at a low frequency (or high temperature) in the sand asphalt mixture might be due to contact stresses between sand particles, although the reason is not definitely conclusive yet. Aging clearly increases the material stiffness in both the length scales.

4.3 Prony Series Representation

The Prony series representation of the viscoelastic materiel properties has been widely used by many researchers. Its advantage lies in the fact that it allows for easy and effective means of converting one material property such as relaxation modulus to another property such as creep compliance. In the present section, the material properties in the form shown in Equations (4.5) and (4.6) are obtained for both length scales (i.e., binder and sand asphalt mixture). The methodology adopted is similar to that described by Schapery [18].

In order to completely represent the properties in the form shown in Equation (4.5), several parameters need to be obtained (G_∞, G_i and ρ_i) from experimental data. Since the experiment performed is in the frequency domain, the form shown in Equations (4.9) and (4.10) are used. The number of collocation points typically depends on the number of decades of the experimental data span in the log frequency domain. As illustrated in Figure 4.13, for an unaged binder, nine collocation points were chosen with the nine-decade data span. This collocation method is used for obtaining linear viscoelastic properties in the form of Prony series parameters (G_∞, G_i and ρ_i) through a system of linear equations until a smooth fit is obtained for the

storage modulus (G'), loss modulus (G''), and dynamic modulus (|G*|), as shown in Figure 4.13 and Figure 4.14.

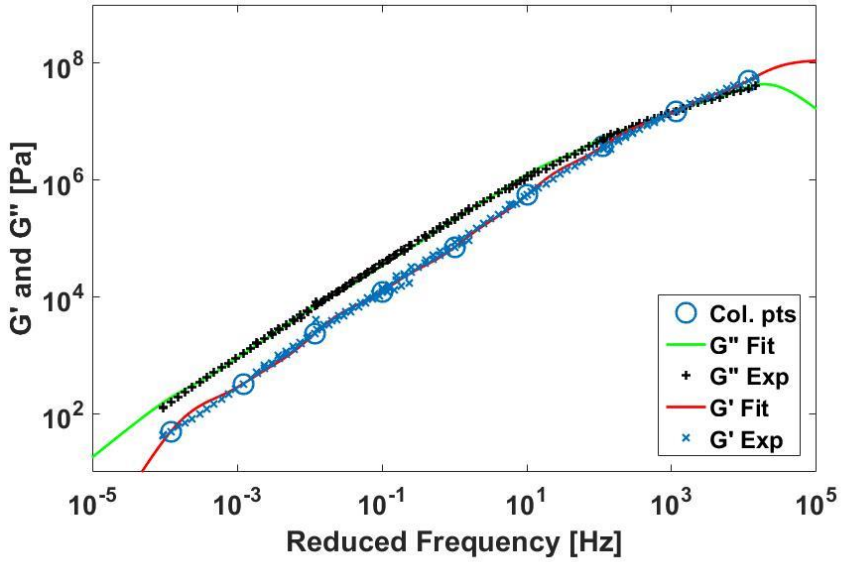

Figure 4.13 Prony fit to experimetal G' and G'' for unaged binder

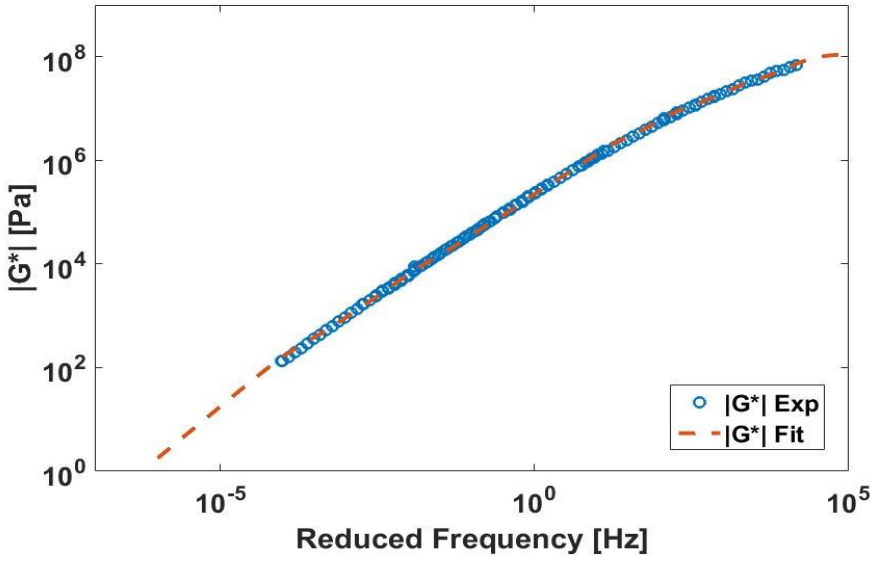

.

Figure 4.14 Prony fit to experimental |G*| for unaged binder

Once the material properties in the form shown in Equation (4.4) are obtained, they can be converted to define other properties such as creep compliance. Figure

4.15 shows the creep compliance converted from the relaxation modulus using the Prony series parameters fitting the frequency domain data. Since binder is mostly modelled as a viscoelastic liquid, G_∞ is zero and has a positive η_o value.Figure 4.16 shows the |J*| fit using the parameters obtained in the conversion process.

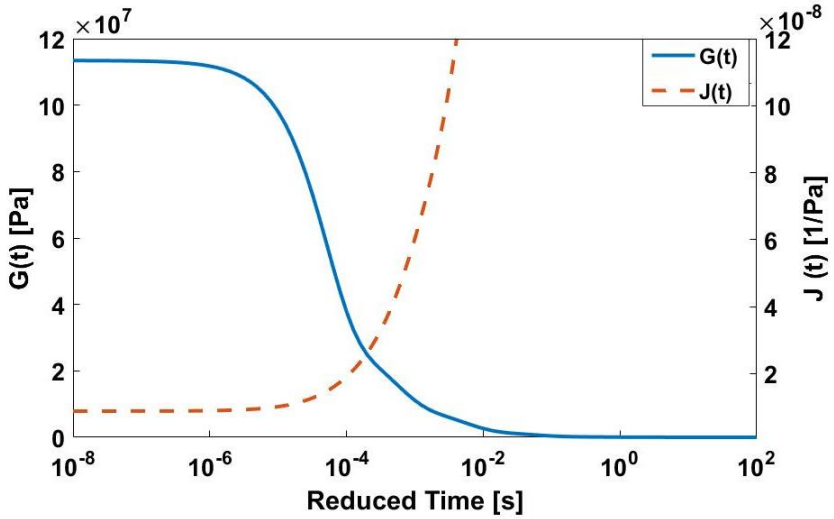

Figure 4.15 G(t) and J(t) prony series plots for unaged binder

.

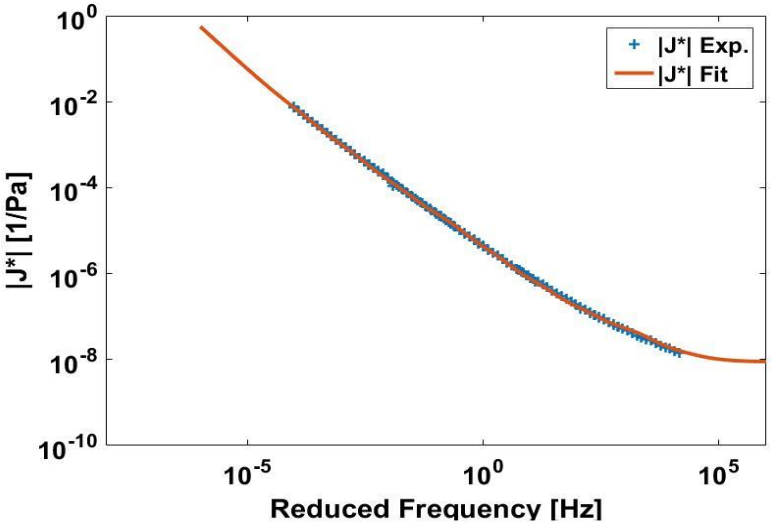

Figure 4.16 Prony fit to experimental |J*| for unaged binder

The prony parameters describing the G(t) and J(t) are shown in Table 4.6 for binder under unaged, RTFOT aged and PAV aged conditions.

Table 4.6 Prony series parameters for unaged binder

Unaged				
No. of Prony terms	ρ_i	G_i	τ_i	J_i
1	5.00E-05	8.29E+07	6.00E-05	3.64E-09
2	0.0005	2.08E+07	0.0006	3.39E-08
3	0.005	7.87E+06	0.006	6.71E-08
4	0.05	1.68E+06	0.06	2.59E-07
5	0.5	1.72E+05	0.6	1.20E-06
6	5	2.56E+04	6	1.00E-05
7	50	6.27E+03	60	4.34E-05
8	500	4.79E+02	600	3.33E-04
9	5000	1.75E+02	6000	1.54E-03
			J_g	8.82E-09
			η_0	1.78E+06
RTFOT aged				
No. of Prony terms	ρ_i	G_i	τ_i	J_i
1	7.00E-05	7.96E+07	8.40E-05	3.51E-09
2	0.0007	3.34E+07	0.00084	1.98E-08
3	0.007	1.15E+07	0.0084	4.87E-08
4	0.07	3.66E+06	0.084	1.58E-07
5	0.7	7.29E+05	0.84	6.90E-07
6	7	1.66E+05	8.4	2.77E-06

7	70	2.77E+04	84	1.20E-05
8	700	4.07E+03	840	7.91E-05
9	7000	1.04E+03	8400	2.64E-04
			J_g	7.75E-09
			η_0	1.41E+07
		PAV aged		
No. of Prony terms	ρ_i	G_i	τ_i	J_i
1	0.0001	5.22E+07	0.00012	4.22E-09
2	0.001	2.95E+07	0.0012	1.70E-08
3	0.01	1.53E+07	0.012	3.14E-08
4	0.1	4.92E+06	0.12	1.30E-07
5	1	1.35E+06	1.2	4.33E-07
6	10	3.80E+05	12	1.39E-06
7	100	6.31E+04	120	6.81E-06
8	1000	1.42E+04	1200	3.35E-05
9	10000	3.32E+03	12000	8.86E-05
			J_g	9.65E-09
			η_0	5.96E+07

A similar approach used for binder samples was adopted for the sand asphalt mixture samples. It should be noted that sand asphalt mixtures were modeled as linear viscoelastic solid-like material, while asphalt binder samples were assumed as linear viscoelastic fluid-like material. Figure 4.17 shows the Prony series fit for shifted storage and loss modulus master curves, and Figure 4.18 shows the shear relaxation

modulus and creep compliance for the unaged sand asphalt mixture sample. Similar analysis was performed for RTFOT and PAV aged sand asphalt samples..

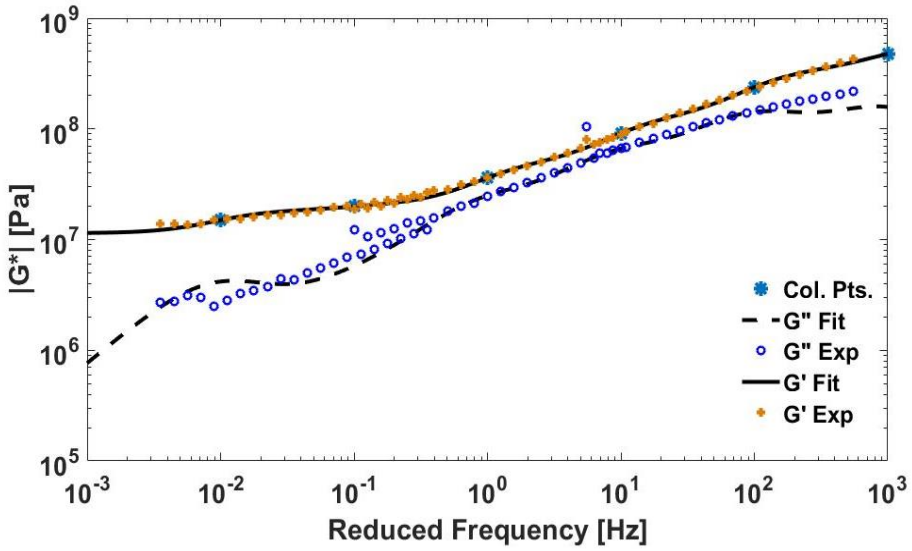

Figure 4.17 Prony fit for storage and loss modulus using frequency sweep data for unaged sand asphalt

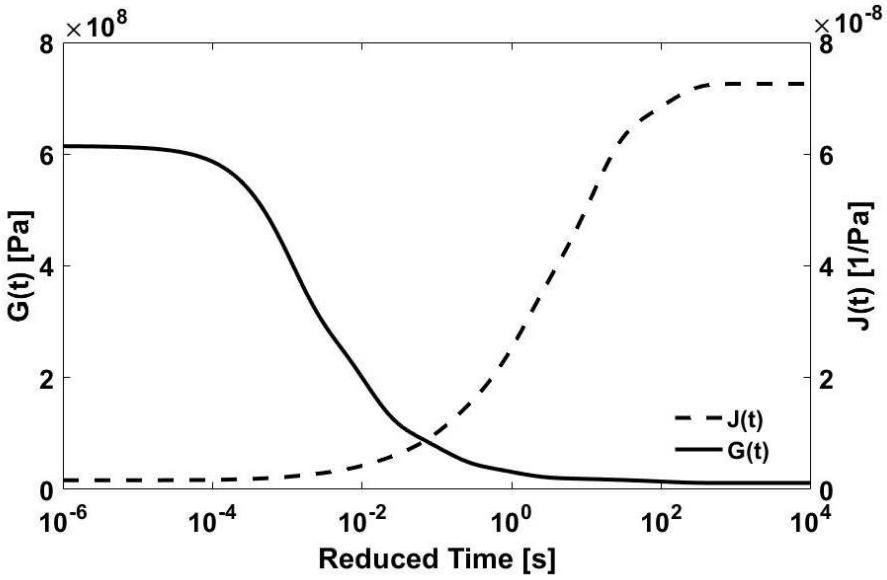

Figure 4.18 G(t) and J(t) obtained for unaged sand asphalt

The resulting Prony series parameters fitted for sand asphalt samples are shown in Table 4.7.

Table 4.7 Prony series parameters for sand asphalt mixture

Unaged				
No. of Prony terms	ρ_i	G_i	τ_i	J_i
1	1.00E-03	2.71E+08	1.10E-03	6.24E-10
2	0.01	2.15E+08	0.011	2.02E-09
3	0.1	7.91E+07	0.11	6.54E-09
4	1	2.89E+07	1.1	1.95E-08
5	10	2.39E+06	11	3.22E-08
6	100	7.09E+06	110	1.01E-08
	G_∞	1.14E+07	J_g	1.63E-09
RTFOT aged				
No. of Prony terms	ρ_i	G_i	τ_i	J_i
1	4.00E-03	3.29E+08	4.12E-03	8.61E-10
2	0.04	1.46E+08	0.0412	2.74E-09
3	0.4	6.24E+07	0.412	5.67E-09
4	4	2.05E+07	4.12	7.08E-09
5	40	7.20E+06	41.2	3.32E-09
6	400	6.37E+06	412	3.26E-09
	G_∞	7.13E+06	J_g	1.73E-09

PAV aged				
No. of Prony terms	ρ_i	G_i	τ_i	J_i
1	4.00E-03	3.37E+08	4.12E-03	6.84E-10
2	0.04	1.82E+08	0.0412	1.95E-09
3	0.4	8.64E+07	0.412	4.26E-09
4	4	3.01E+07	4.12	6.43E-09
5	40	1.04E+07	41.2	3.81E-09
6	400	8.40E+06	412	3.36E-09
	G_∞	7.96E+06	J_g	1.51E-09

CHAPTER FIVE

FATIGUE DAMAGE CHARACTERIZATION IN BINDER AND SAND ASPHALT

5.1 Introduction

Fatigue in asphalt concrete has been of interest for many decades. It is one of the most important forms of distress in pavement leading to top-down and/or bottom-up cracking.

By applying Schapery's [16] extended elastic-viscoelastic correspondence principle, which allows for the separation of viscoelastic effects from damage, one can reduce the viscoelastic problem to a corresponding elastic problem by replacing the physical strains during the test with pseudo-strain γ^R, as defined in Equation (5.1).

$$\gamma^R = \frac{1}{G_r} \int_0^{t_R} G(t_R - \zeta) \frac{d\gamma}{d\zeta} \, d\zeta \tag{5.1}$$

$G(t)$, t_R, and ζ are shear relaxation modulus, reduced time, and time variable for integration, respectively. G_R is an arbitrary reference modulus usually taken to be a unity. Based on the linear viscoelastic response, one can write the shear stress in the form shown in Equation (5.2). Using the relation in Equation (5.1), Equation (5.2) can be rewritten as Equation (5.3), which is similar to the linear elastic hook's law.

$$\tau = \int_0^{t_R} G(t_R - \zeta) \, {}^{d\gamma}/_{d\zeta} \, d\zeta \tag{5.2}$$

$$\tau = G_R \gamma^R \tag{5.3}$$

In order to quantify the macroscale observations of damage evolution, a simple parameter (pseudo stiffness) can be considered as shown in Equation (5.4). $C(S)$ is the pseudo stiffness which is dependent on the internal damage parameter *S*.

$$C(S) = \frac{\tau}{\gamma^R} \tag{5.4}$$

Using sinusoidal loading, Equations (5.1) and (5.4) can be written in the oscillatory mode. For viscoelastic materials subjected to sinusoidal loading, one can see hysteresis loops when plotting the strain vs. stress. The area under the loop accounts for the energy dissipation within the material. When the extended elastic-viscoelastic correspondence principle formulated by Schapery [16] is applied, the hysteresis disappears, and a linear relation exists between the pseudo strain and stress. The peak pseudo strain is defined as follows in Equation 5.5, and peak pseudo stiffness is defined in Equation (5.6). Safaei et al. [19] suggested the use of D.M.R, which is defined as the ratio of the initial dynamic modulus of the sample during fatigue testing at very low levels of strain divided by the linear viscoelastic dynamic modulus of the material. This accounts for sample-to-sample variability during testing.

$$\gamma_p^R = \frac{1}{G_R}\left(\gamma_p|G^*_{LVE}|(\omega_R)\right) \tag{5.5}$$

$$C^*(S) = \frac{\tau_p}{\left(\gamma_p^R \times D.M.R\right)} \tag{5.6}$$

The fundamental approach adopted in the simplified viscoelastic continuum damage (S-VECD) characterization of damage is based on Schapery's work potential

theory [16], which is based on the thermodynamics of irreversible processes. The damage evolution law proposed by Schapery is provided in Equation (5.7), where W^R is the stored pseudo strain energy, *S* is the internal state variable that represents the damage parameter, and α is a material parameter that describes the rate of damage evolution.

$$\frac{dS}{dt} = \left(-\frac{\partial W^R}{\partial S}\right)^{\alpha} \tag{5.7}$$

$$W^R = \frac{1}{2} C^*(S)\left(\gamma_p^R\right)^2 \tag{5.8}$$

The value of C^* is a material indicator, which is 1.0 when there is no damage or is within the linear viscoelastic regime. As the material accumulates damage, the peak pseudo stiffness (C^*) begins to drop, indicating loss in material integrity, and the material loses its ability to store pseudo strain energy. Using Equations (5.5) through (5.8), one can arrive at an analytical equation for *S*, as shown in Equation (5.9), and establish a unique relationship between C^* and S, as shown in Equation (5.10). This relation is called the damage characteristic curve because it is unique for a given material, and it is independent of the type, mode, and temperature of loading [19].

$$S = \sum_{i=1}^{N} \left[D.M.R/_2 \left(\gamma_{p,i}^R\right)^2 \left(C_{i-1}^* - C_i^*\right)\right]^{\alpha/(1+\alpha)} \left[t_i - t_{i-1}\right]^{1/(1+\alpha)} \tag{5.9}$$

$$C^* = 1 - C_1(S)^{C_2} \tag{5.10}$$

5.2 Experimental Investigation

To characterize fatigue damage, several tests were performed in oscillatory mode on binder and sand asphalt mixture samples under a multitude of conditions. The idea was to incorporate the effects of temperature, loading rate (frequency), stress, strain, and the influence of aging on the fatigue resistance of samples. The entire test matrix is provided in Table 5.1 for the binder, and in Table 5.2 for the sand asphalt mixture.

Table 5.1 Fatigue test matrix for binder

Aging	Time Sweep (Controlled Strain)	Time Sweep (Controlled Stress)	Strain Sweep
Unaged	3%, 4%, 5%	50 kPa	LAS-1 (25, 20, 15 °C), LAS-2
RTFOT	3%, 4%, 5%	75kPa	LAS-1 (25, 20, 15 °C), LAS-2
PAV	4%, 5%, 6%	-	LAS-1 (25, 20, 15 °C), LAS-2

Table 5.2 Fatigue test matrix for sand asphalt mixture

Aging	Time Sweep (Controlled Strain)	Strain Sweep
Unaged	0.2%, 0.25%, 0.35%	LAS-2 (25 °C)
RTFOT	0.25%, 0.35%,0.45%	LAS-2 (25 °C)
PAV	0.2%, 0.25%, 0.3%	LAS-2 (25 °C)

The LAS-1 is the most recent AASHTO TP 101 standard that is currently being used for binder fatigue tests. LAS-2 is another form of the strain sweep test where the only difference compared to LAS-1 is that the strain is increased in the logarithmic mode in LAS-2.

5.3 Fatigue Failure Criterion

It is important to clearly define the failure point and failure criterion for the analysis of fatigue damage and the use of S-VECD analysis. Several researchers have extensively investigated the definition of the failure point in the asphalt concrete and binder. The simplest definition of the fatigue failure point is a 50% reduction in stiffness. However, due to the arbitrary nature of its definition, it has been constantly challenged. Energy-based criterion were developed later to overcome the 50% reduction in the stiffness definition. This approach was more promising due to its more fundamental nature and its ability to describe marked changes in the material behavior due to the damage evolution. For most bituminous materials one can observe a hysteresis loop when plotting a stress vs. strain curve during sinusoidal loading. Similar observations can be seen in the binder and sand asphalt mixture as it is a consequence of the viscoelastic nature of the material. The area under the hysteresis loop is the dissipated energy in the material. Based on the dissipated energy concept two definitions of fatigue failure criterion emerged. The Dissipated Energy Ratio (DER) and the Ratio of Dissipated Energy Change (RDEC) have been successfully applied to the asphalt binder and the asphalt concrete in order to define the fatigue failure point. Another approach to define the point of failure was attempted by observing the changes in the slope of the stiffness and peak in the phase angle during fatigue tests. This approach clearly identified regions of microcracking, coalesce of mircrocracks, crack propagation, and complete failure or rupture in the material.

Another popular method that has become increasingly used is the peak in C^* x N values during loading cycles. Although phenomenological in approach, this method has been able to capture the trends in fatigue damage evolution in the binder and mixture relatively well. Rowe and Bouldin [20] first applied this criterion to asphalt mixtures and could define fatigue failure successfully. By observing the trends in E^*, they could identify four stages of damage evolution in asphalt concrete under fatigue. The distinct regions were identified as: (1) internal heating, (2) micro-cracking, (3) crack formation/propagation, and (4) sample breakdown. They observed that by mathematically representing E^* as a Taylor series expansion and function of N (Number of cycles) as shown in Equations (5.11) and (5.12), where E^* is stiffness or modulus and E_o^* is the initial stiffness or modulus, the higher order terms were neglected as they did not contribute much when compared to the initial terms.

$$E^* = E_o^* + N\,\frac{\mathrm{d}E^*}{\mathrm{d}N} + \frac{N^2}{2!}\frac{d^2E^*}{dN^2} + \cdots \ldots \ldots \tag{5.11}$$

$$E^*N = E_o^*N + N^2\,\frac{\mathrm{d}E^*}{\mathrm{d}N} + \frac{N^3}{2!}\frac{d^2E^*}{dN^2} + \cdots \ldots \ldots \tag{5.12}$$

During the microcracking phase the $\frac{\mathrm{d}E^*}{\mathrm{dN}}$ is constant and negative whereas the second order differential term is zero. When damage accumulation is faster or accelerates after a transition from a steady microcracking phase to a crack-propagation, the second order term becomes negative, thereby reducing the product E^*N. Similar observations were made by Kim et al. [13] performed fatigue tests on the sand asphalt mixture samples and also assessed the influence of rest periods on fatigue life due to potential damage healing. They concluded that the transition point

in the stiffness and the product G^* x N correlated well with the peak in the phase angle, thereby providing a reasonable means of identifying fatigue life.

Wang et al. [21] conducted a series of time sweep tests under the strain and stress control mode for different binders in the short term aged condition. They evaluated different failure criterion and concluded that phenomenological and dissipated energy criterion provide good indicators of failure when compared to a 50% reduction in stiffness. Also, statistical analysis revealed that the peak in S x N $\left(S = \frac{|G^*|}{|G^*_{initial}|}\right)$, the peak phase angle, and the RDEC criterion provide similar fatigue life predictions. In their analysis, it was observed that, for some polymer modified binders, the phase angle tends to gradually increase without any peaks, and the RDEC criterion was mostly dependent on how the data was interpreted. They concluded that the peak in S x N would be a better indicator of the failure point as it can indicate the rapid growth of damage accumulation. In the current investigation, similar fatigue failure criterion was used by taking the peak in C^* x N ($C^* = Pseudo\ Stiffness$) as defined by Safaei et al. [19].

Figure 5.1 and 5.2 show results of the time sweep test performed at 4% strain amplitude for the unaged binder sample. In this case, it can be seen that C^* x N did not show a peak value but a clear transition in the slope of the C^* x N curve. This trend was also observed even in the RTFOT aged binder samples, as shown in Figure 5.6.

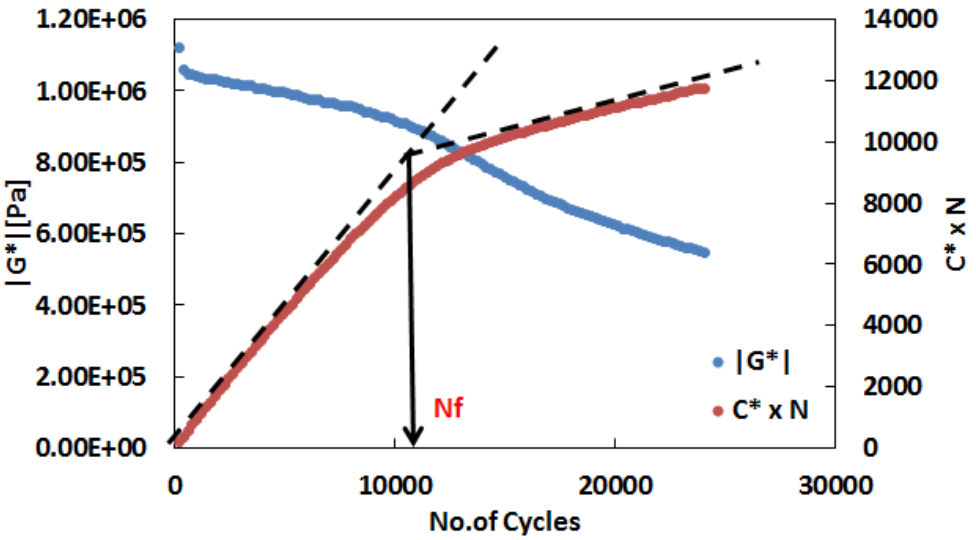

Figure 5.1 |G*| and C* x N vs No. of cycles in time sweep test for unaged binder at 5% strain

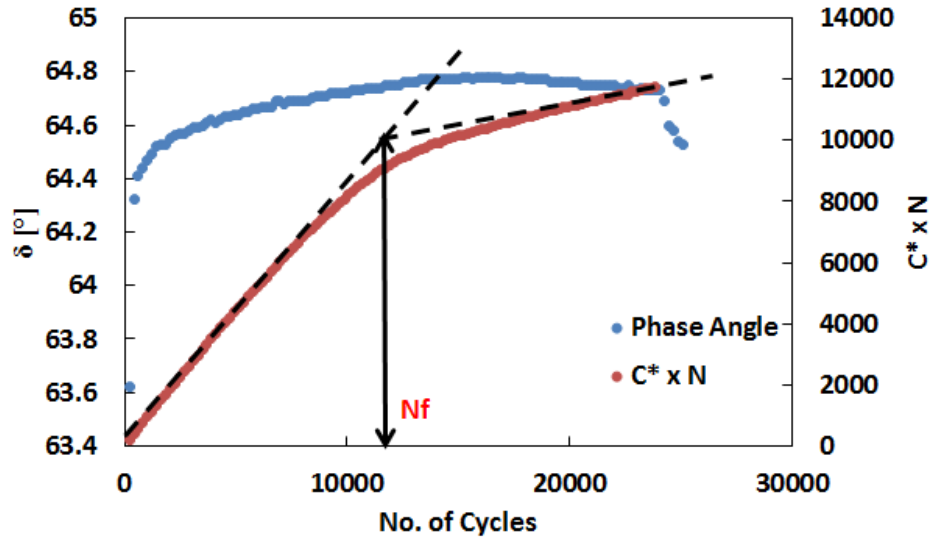

Figure 5.2 Phase angle and C* x N vs no. of cycles in time sweep test for unaged binder at 5% strain

In controlled stress time sweep tests, a different trend in |G*| and phase angle values were observed relative to controlled strain time sweep tests. This difference can be attributed to the mode of loading. In the case of controlled strain tests, the

stress within the sample reduces as damage accumulates, meaning it takes less effort to deform to a particular state once the sample has experienced significant damage. On the other hand, in controlled stress tests, the sample is subjected to a constant level of stress, meaning that the sample has to undergo large deformation once there is significant damage to maintain the same level of stress. This is clearly observed in Figure 5.3 and Figure 5.4, where there is a phase of steady decrease in $|G^*|$ values and an increase in the phase angle. Once the transition point or the peak in the C^* x N curve occurs, there is a faster rate of drop in the $|G^*|$ value and a corresponding increase in the phase angle, which indicates faster damage accumulation (such as crack propagation). The trend observed in Figure 5.3 and Figure 5.4 was consistently across RTFOT and PAV aged samples. This shows that controlled stress time sweep tests are capable of phases of radially oriented crack formation and propagation.

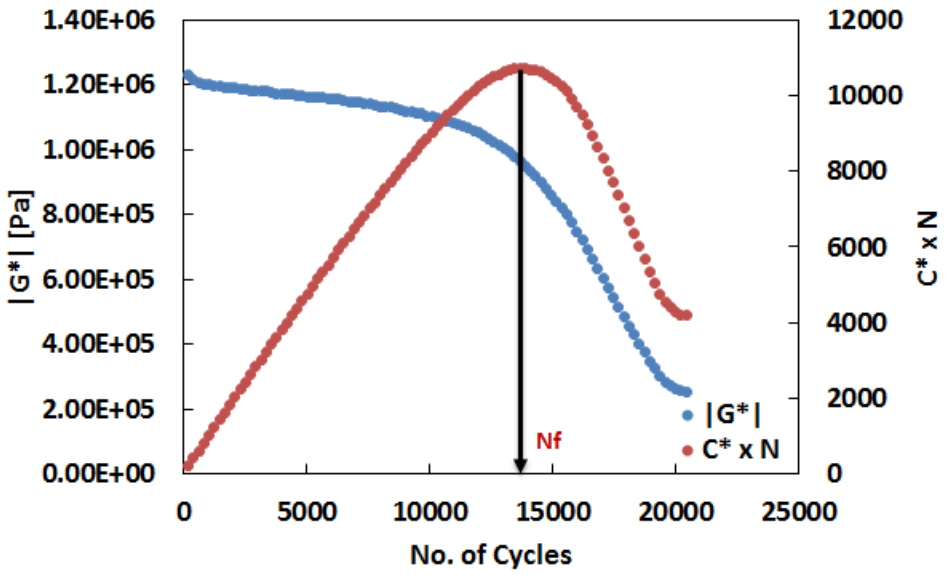

Figure 5.3 |G*| and C* x N vs N in time sweep test for unaged binder at 50 kPa stress

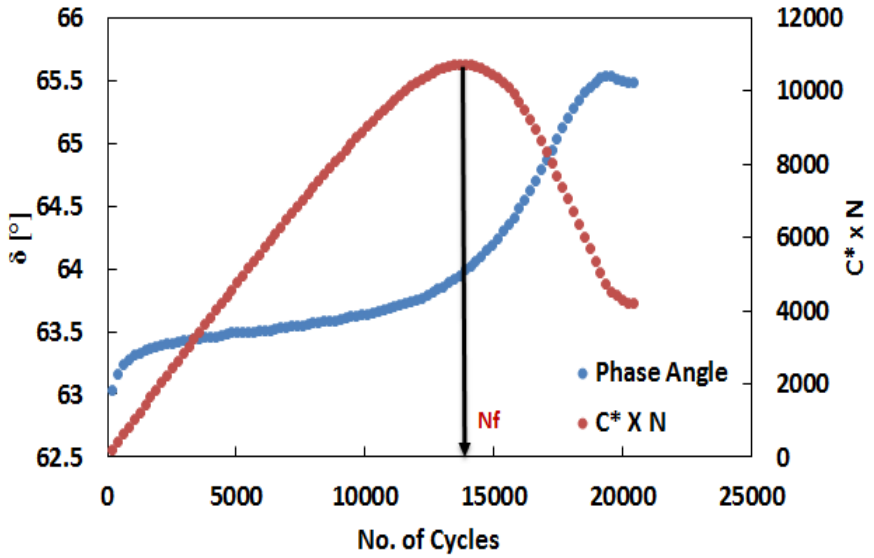

Figure 5.4 δ and C* x N vs N in time sweep test for unaged binder at 50 kPa strain

Similar trends for |G^*| and δ were observed for the RTFOT aged binder, as shown in Figure 5.5 and Figure 5.6.

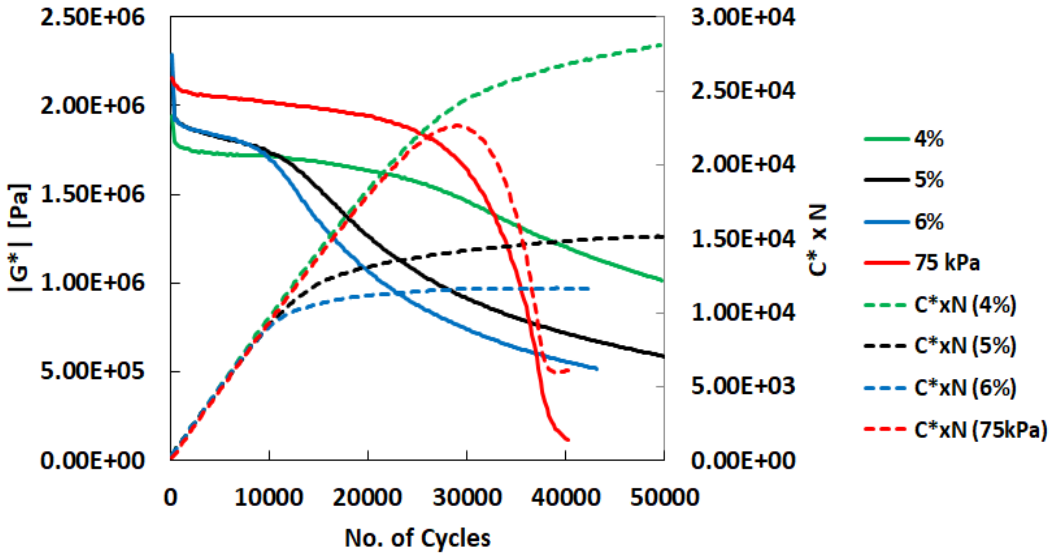

Figure 5.5 |G*| and C* x N values in time sweep tests for RTFOT aged binder

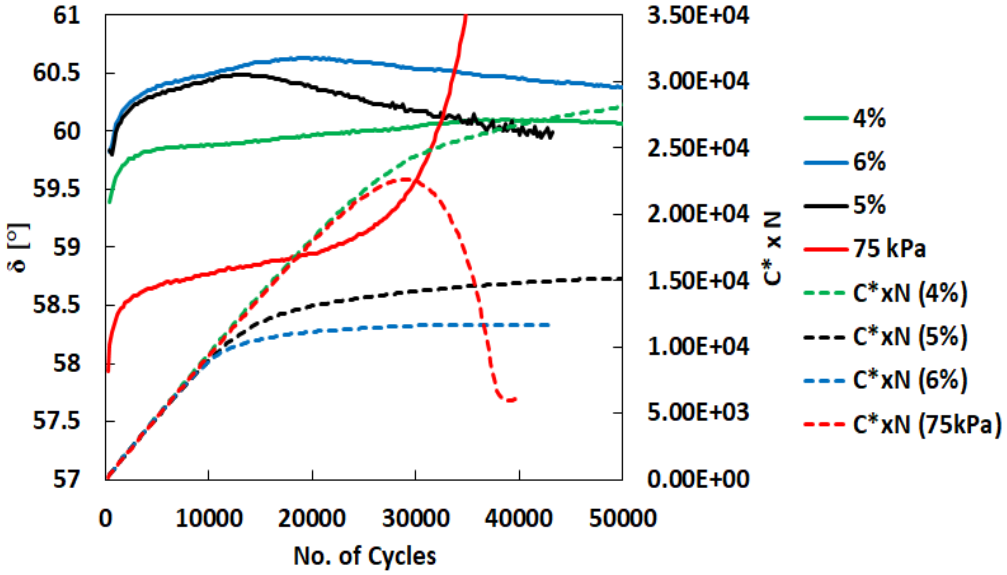

Figure 5.6 δ and C*xN vs N in time sweep test for RTFOT aged binder

Unlike in unaged and RTFOT aged binder samples, there was a clear correlation with the peak in C^* x N, drop in $|G^*|$ values, and peak in the phase angle for the PAV aged binder, as shown in Figure 5.7 and Figure 5.8. The peak in the phase angle was a clear indication of fatigue failure due to damage, as shown in Figure 5.8.

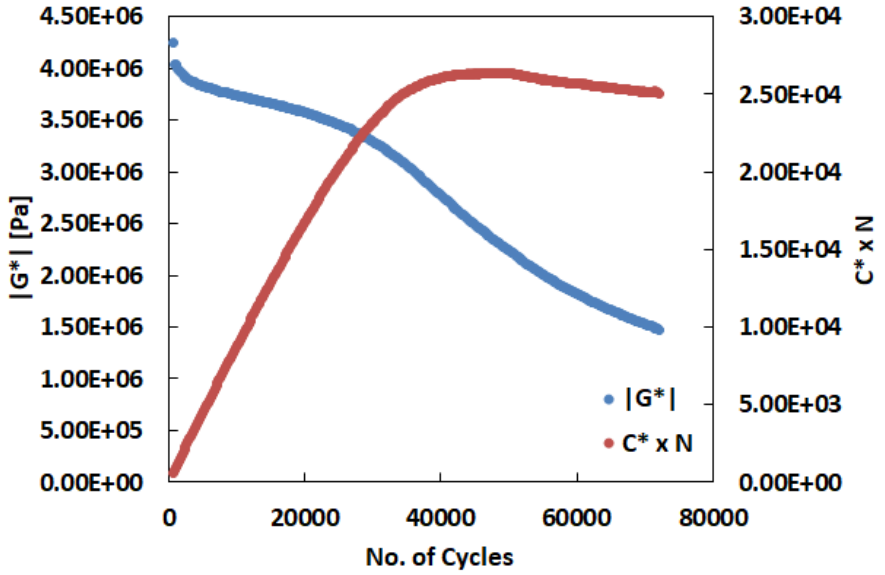

Figure 5.7 |G*| and C*xN vs N in time sweep test at 7% strain ampltude for PAV aged binder

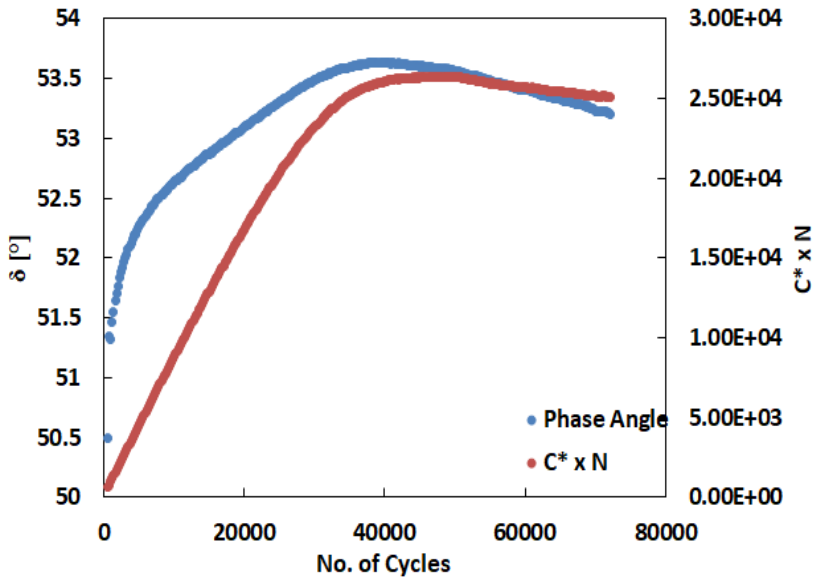

Figure 5.8 δ and C*xN vs N in time sweep at 7% strain amplitudetest for PAV aged binder

The time sweep test conducted on an unaged sand asphalt mixture sample is exemplified in Figure 5.9. It shows the phase of micro-cracking where there is a steady increase in the phase angle and a steady decrease in the $|G^*|$ value. This phase is succeeded by a transition point beyond which there is an increased rate of damage accumulation. This region in the fatigue test can be called the macrocracking phase. During the macrocracking phase one can notice the faster rate of decrease for the $|G^*|$ value and a simultaneous increased rate of the phase angle growth. At the end of the fatigue test the sample breaks apart completely, which is associated with the sudden drop in the phase angle.

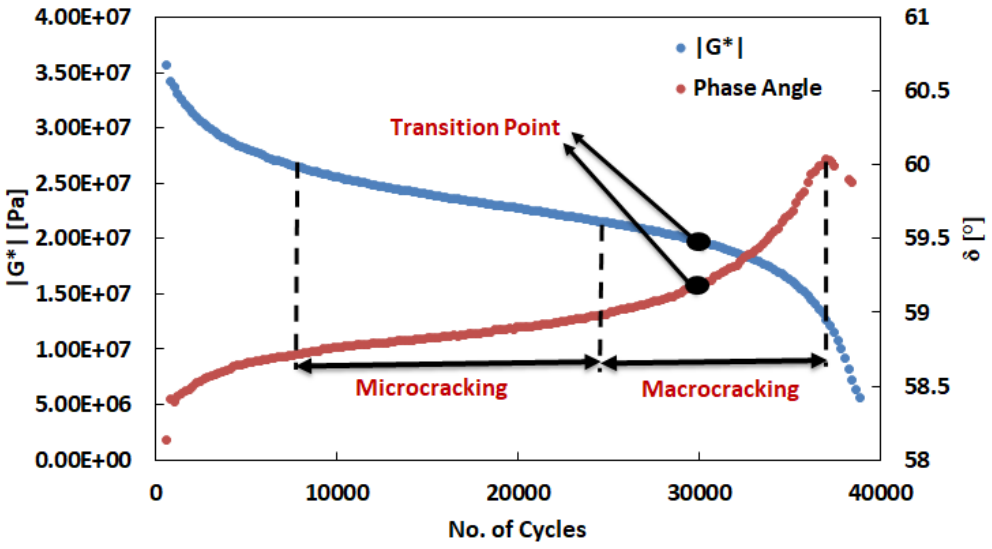

Figure 5.9 |G*| and δ for time sweep test at 0.25 % strain amplitude for unaged sand asphalt mixture identifying micro and macro cracking

For the unaged sand asphalt sample, the time sweep test performed at a strain amplitude of 0.35% is shown in Figure 5.10 and Figure 5.11. It can be observed that the peak in C^* x N correlated well with the fatigue damage, as confirmed by the rapid decrease of $|G^*|$ and the increase of the phase angle. Unlike the binder, there was no

ambiguity in defining fatigue failure. This is clearly an advantage associated with the use of the sand asphalt mixture samples. A similar trend is observed in the case of the RTFOT aged sand asphalt samples, as shown in Figure 5.12 and Figure 5.13. It is important to point out here that the trends observed for the unaged and the RTFOT aged sand asphalt mixture samples were similar to that observed during the stress controlled strain sweep test of the binder.

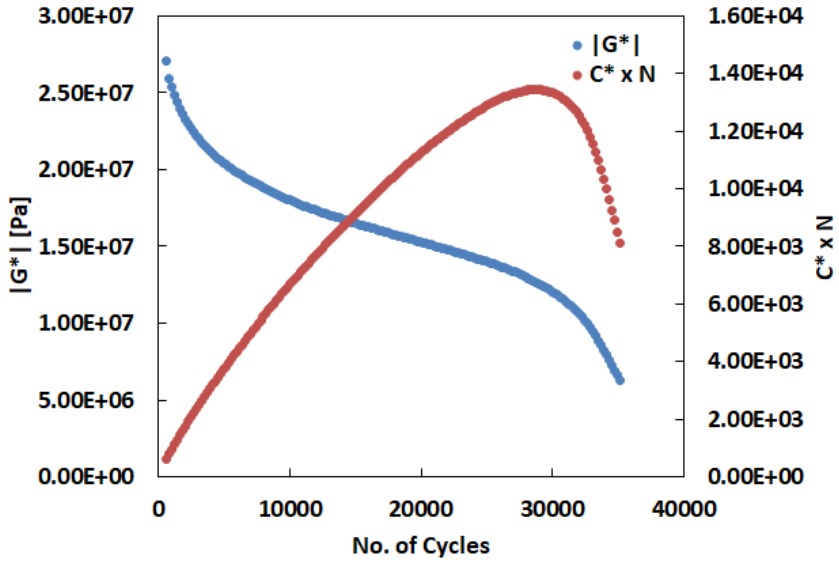

Figure 5.10 |G*| and C* x N vs N for time sweep test at 0.35 % strain amplitude for unaged sand asphalt mixture sample

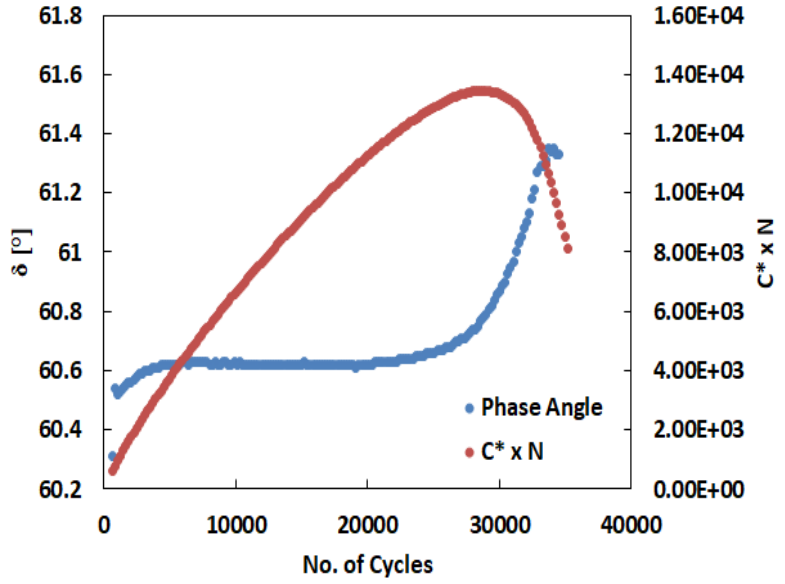

Figure 5.11 δ and C*x N vs N for time sweep test at 0.35% strain amplitude for unaged sand asphalt mixture sample

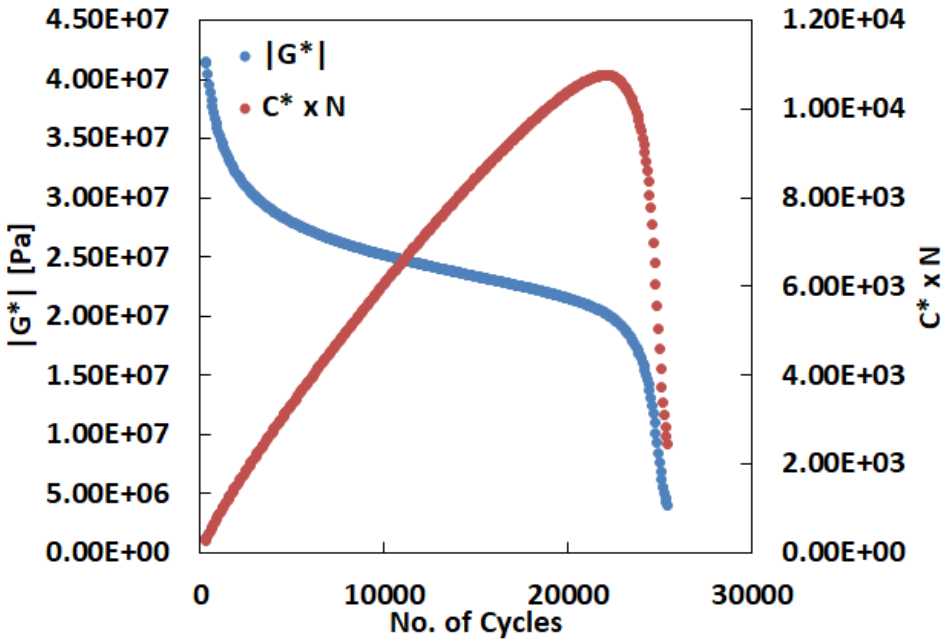

Figure 5.12 |G*| and C*xN vs N for time sweep test at strain amplitude of 0.35% for RTFOT aged sand asphalt mixture sample

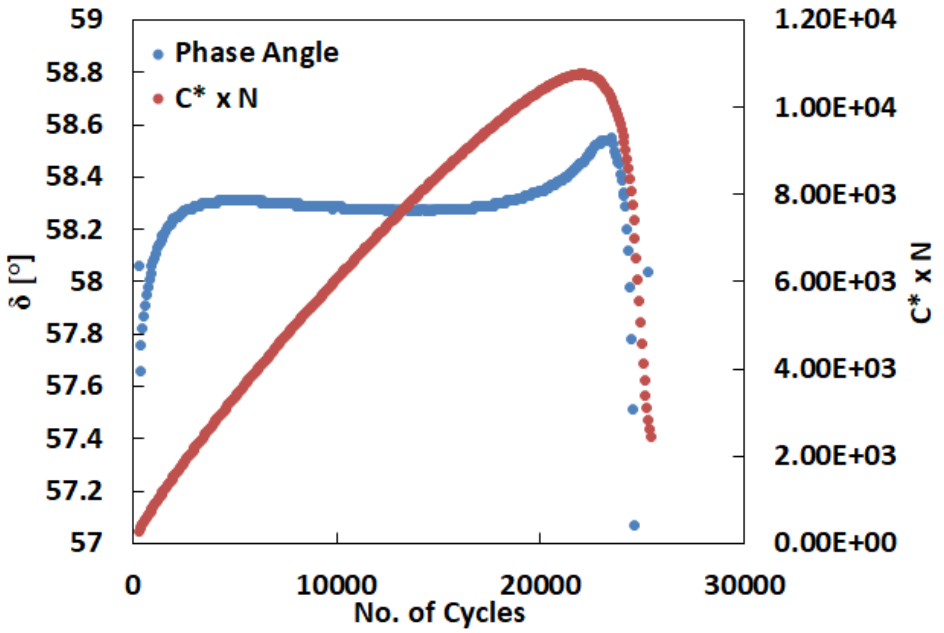

Figure 5.13 δ and C*x N vs N for time sweep test at a strain amplitude of 0.35% for RTFOT aged sand asphalt mixture sample

In the case of the PAV aged sand mixture, there was no increase in the phase angle after the peak in the *C** x *N* value. It showed a sudden drop of the phase angle which indicates fatigue failure, as shown in Figure 5.14 and Figure 5.15. This implies less macrocracking phase before a complete failure in the PAV aged mixture samples compared to unaged and RTFOT aged samples. The sudden drop in stiffness and the phase angle indicates that a transition from microcracking to complete failure was accelerated in the case of the PAV aged samples.

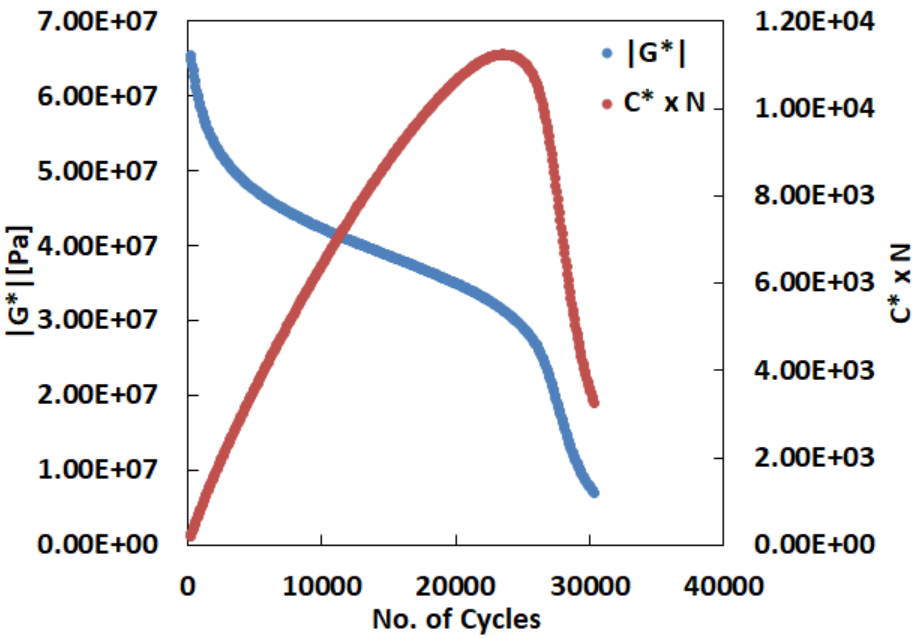

Figure 5.14 |G*| and C*x N vs N for time sweep test at strain amplitude of 0.25% for PAV aged sand asphalt mixture sample

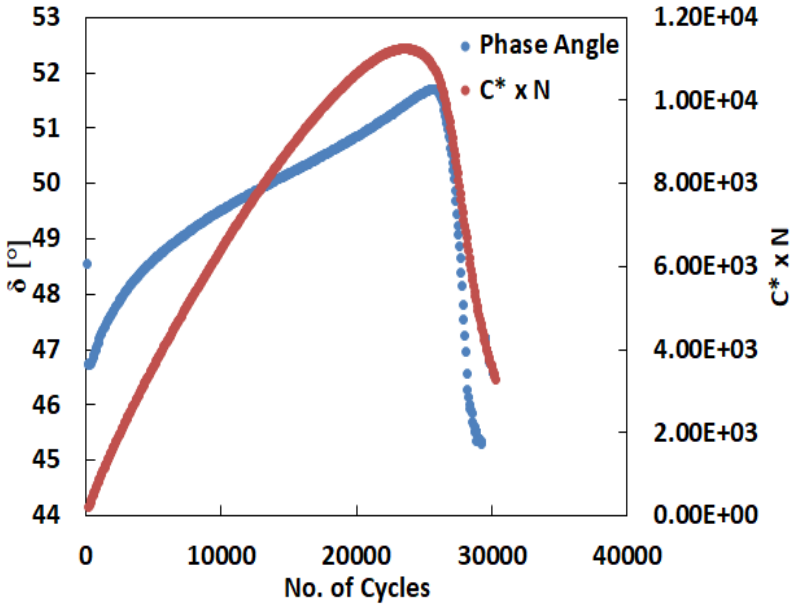

Figure 5.15 δ and C*x N vs N for time sweep test at strain amplitude of 0.25% for PAV aged sand asphalt mixture sample

Figure 5.16 through Figure 5.18 show the time sweep test results in the form of fatigue life vs. strain amplitude for the unaged, RTFOT aged, and PAV aged binder samples. The fatigue life (i.e., the number of cycles to failure (N_f)) in the fatigue tests are based on the peak in C^* x N values. It can be observed that with an increase in the strain amplitude, there is a decrease in fatigue life, which is expected and consistent across different aging conditions.

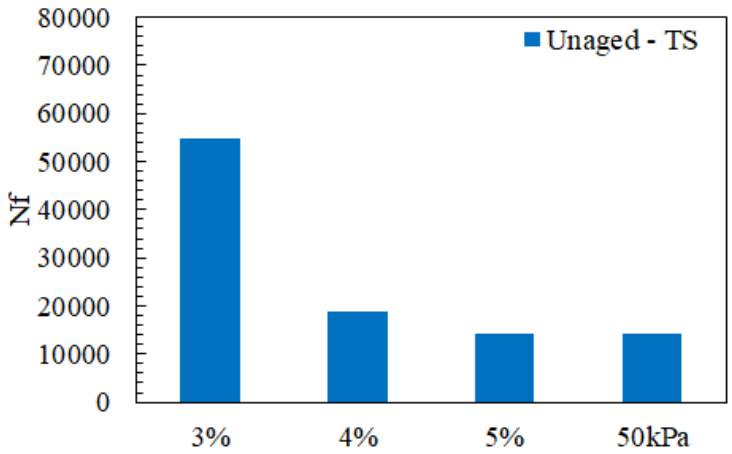

Figure 5.16 N_f for different strain/stress amplitudes in time sweep tests performed on unaged binder

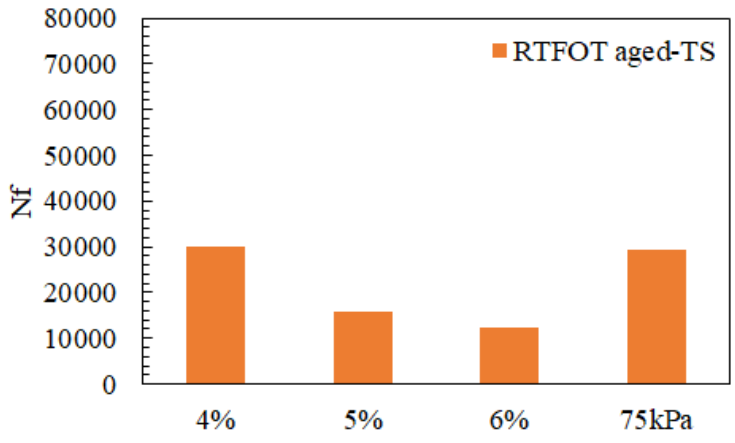

Figure 5.17 N_f for different stress/strain amplitudes in time sweep tests performed on RTFOT aged binder

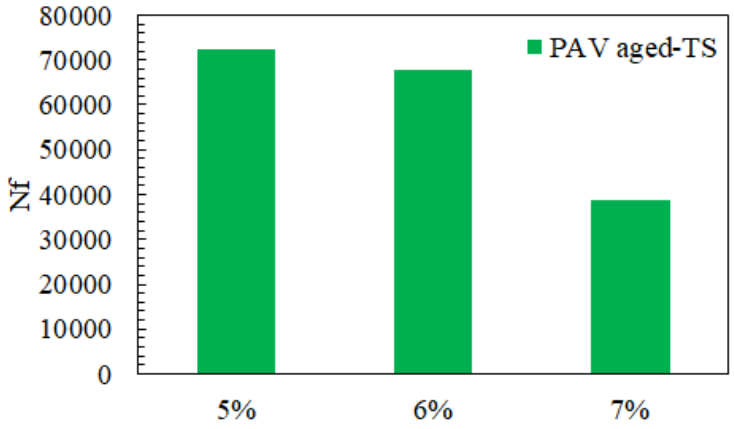

Figure 5.18 N_f for different strain amplitudes in time sweep tests performed on PAVaged binder

Figure 5.19 shows the fatigue life for LAS-1 tests performed on the unaged, RTFOT aged, and PAV aged binder at different testing temperatures. It can be observed that the fatigue life reduces as the temperature decreases irrespective of the aging condition. It is clear that the binder is more susceptible to fatigue cracking at lower temperatures. Moreover, it can be observed that at different temperatures the PAV aged binder shows improved fatigue resistance relative to unaged and RTFOT aged samples. This is in contrast with the general belief that aging is one of the primary reasons responsible for fatigue cracking in asphalt pavements.

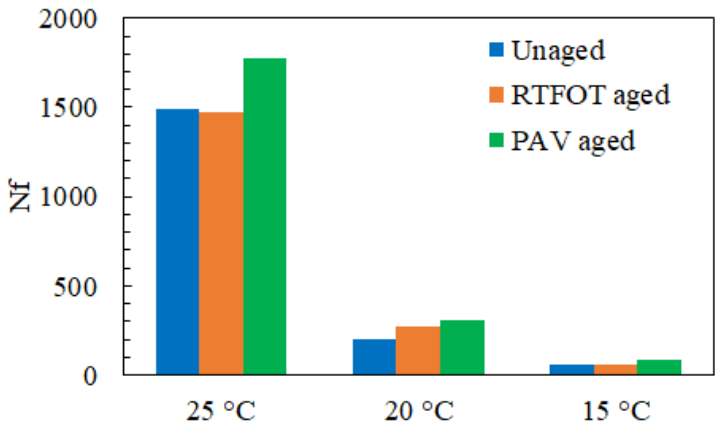

Figure 5.19 N_f for LAS-1 tests at different temperature and aging conditions

Figure 5.20 shows results of time sweep fatigue tests performed at a strain amplitude of 5% and at 25 °C on the unaged, RTFOT aged, and PAV aged binder. It can be observed from the figure and the LAS-1 test results (Figure 5.19) that the influence of aging could not be captured effectively using 2-mm thick binder samples.

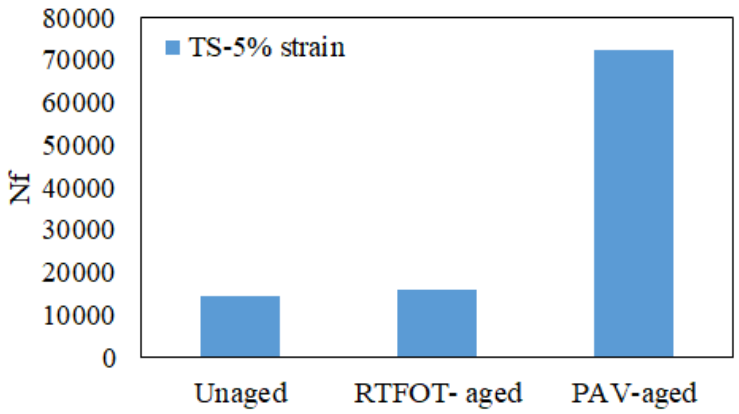

Figure 5.20 N_f for time sweep tests at 5% strain amplitude for different aging conditions

Figure 5.21 through Figure 5.23 show the time sweep test results in the form of fatigue life vs. strain amplitude for the unaged, RTFOT aged, and PAV aged sand asphalt mixture samples.

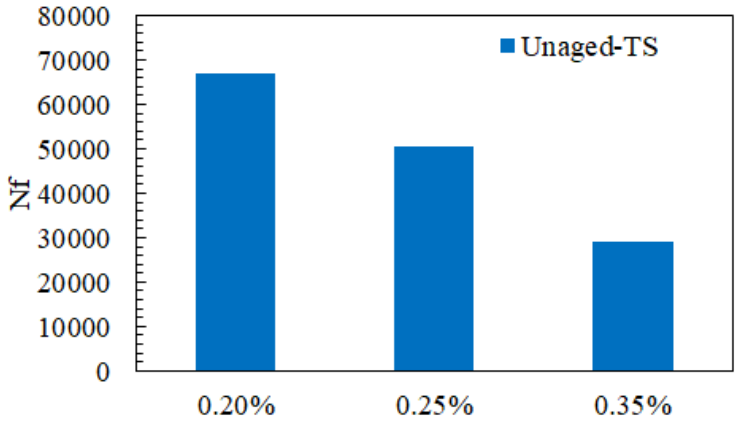

Figure 5.21 N_f for time sweep test at different stain amplitudes for unaged sand asphalt mixture

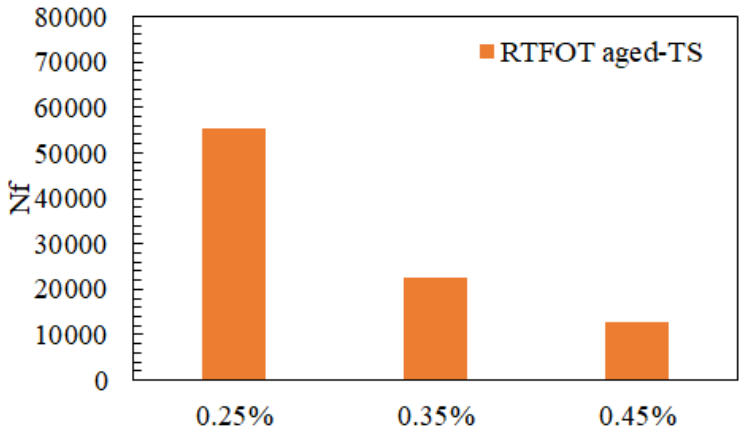

Figure 5.22 N_f for time sweep tests at different strain amplitudes for RTFOT aged sand asphalt mixture

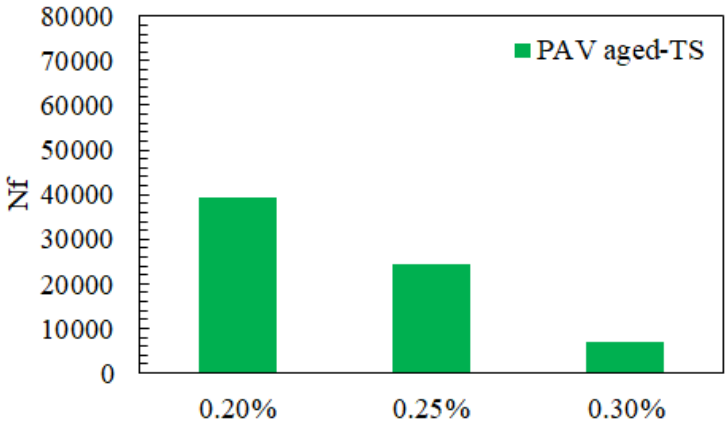

Figure 5.23 N_f for time sweep tests at different strain amplitudes for PAV aged sand asphalt mixture

Figure 5.24 summarizes the time sweep test results at a 0.25% strain amplitude and 25 °C, and Figure 5.25 shows the result from the LAS-2 tests performed for the sand asphalt mixture samples. Both the tests (time sweep and LAS-2) were performed under the three different aging conditions. It can be observed in Figure 5.24 that long

term aging (PAV aging) reduces the fatigue life of the mixture relative to unaged and RTFOT aged conditions. Similar observations can be made in Figure 5.25.

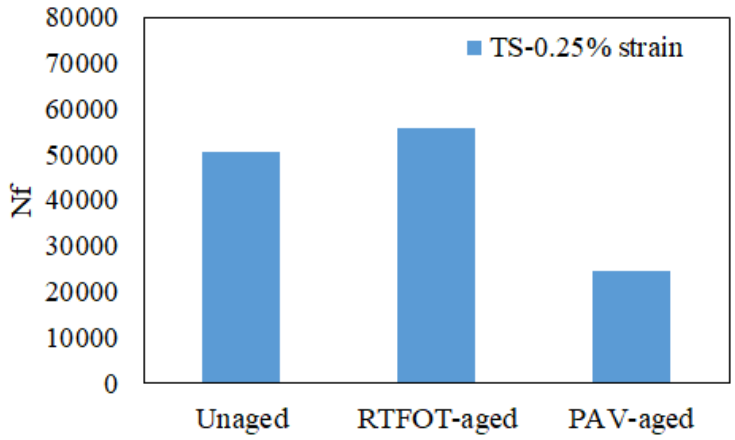

Figure 5.24 N_f for strain sweep tests performed at 0.25% strain amplitude on sand asphalt mixture samples under different aging conditions

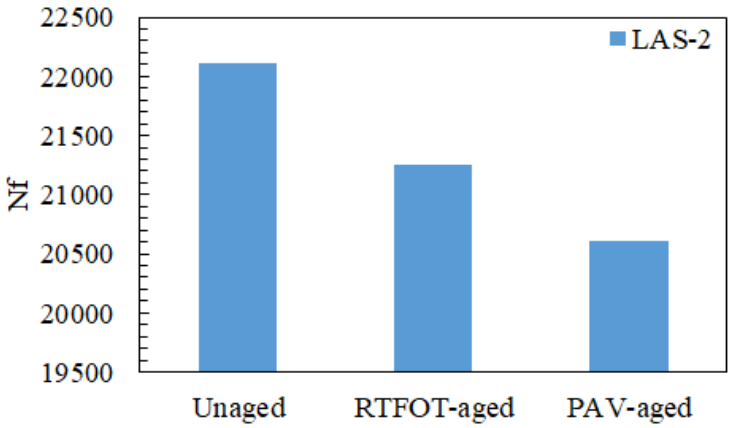

Figure 5.25 N_f for LAS-2 tests on unaged and aged sand asphalt mixture samples

5.4 Damage Characteristic Curve and Fatigue Life

Sabouri et al. [22] came up with an average released pseudo strain energy until failure as a good indicator for incorporating different modes of loading and

temperature effects for asphalt mixtures. They suggested a G^R based failure criterion, where the average pseudo strain energy released until failure versus the number of cycles to failure (N_f) was independent of the type of fatigue test and temperature. Wang et al.(23) suggested the use of peak in pseudo strain energy versus N_f as a good indicator of failure for fatigue testing in binder and based on the work by Sabouri et al.(22) they could expand the application of G^R based analysis to binder. A similar approach was used in this research for both binder and sand asphalt fatigue tests.

Based on the test results, the fatigue failure criterion, and methodology described by Safaei et.al [19], damage characteristic curves were developed for the binder, as shown in Figure 5.26. The damage characteristic curves are material dependent and independent of the type of loading, hence the time sweep data performed at different strain levels should still yield a similar damage curve. By using Equations (5.9) and (5.10), damage characteristic curves shown in Figure 5.26 can be developed from the time sweep fatigue tests of the unaged binder.

The corresponding damage characteristic curves from the LAS tests (LAS -1 and LAS -2) for the unaged binder are shown in Figure 5.27. It is interesting to note that, even though the same model parameter α was used for obtaining the curves for all the LAS data, damage characteristic curves from the LAS tests differed considerably relative to the time sweep case. It should also be noted that the damage curves at different temperatures were shifted using the principle of TTSP and using the same shift factors that were obtained from the linear viscoelastic master curve. Another thing to be noted from Figure 5.27 is that the damage characteristic curves obtained from different LAS tests (LAS-1 and LAS-2) were quite similar, which further implies that the damage characteristic is not quite dependent of loading modes.

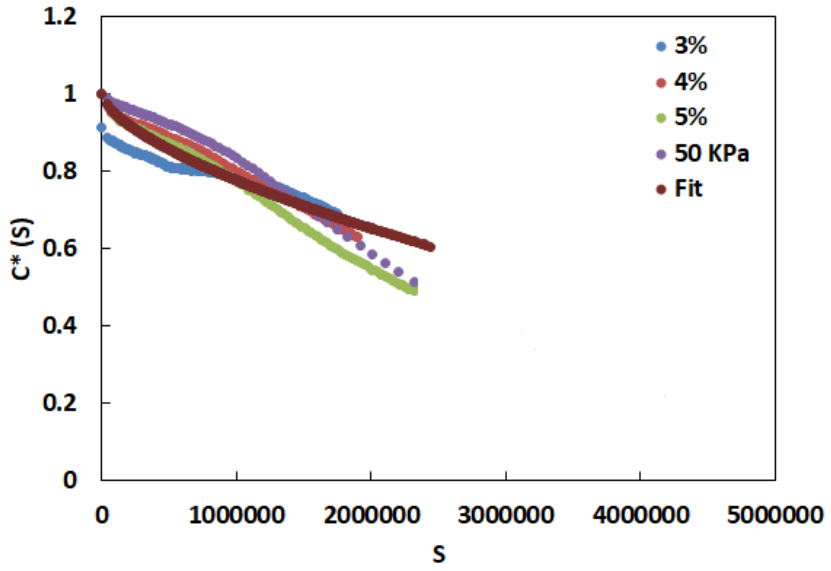

Figure 5.26 Damage chracteristic curve of unaged binder in strain controlled and stress controlled time sweep tests

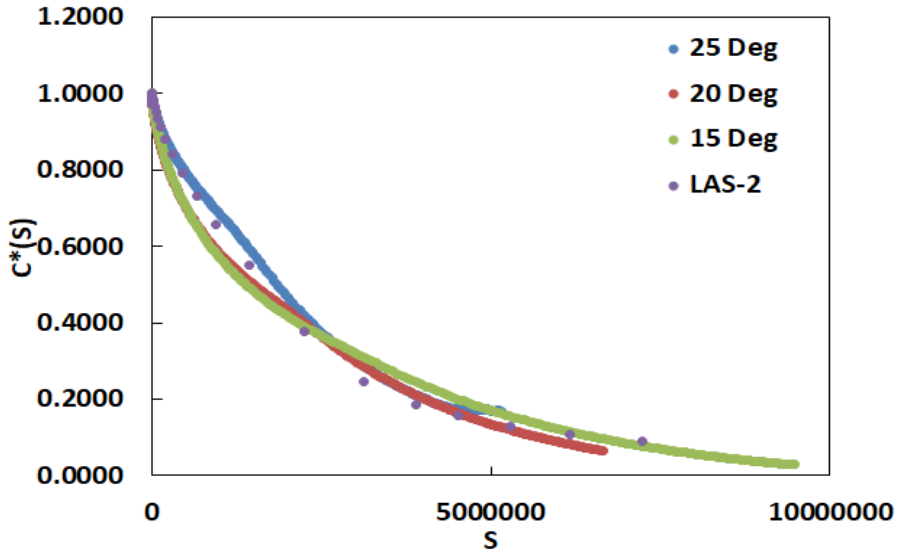

Figure 5.27 Damage chracteristic curve of unaged binder for LAS-1 and LAS-2 tests

Figure 5.28 and Figure 5.29 show the damage characteristic curves for RTFOT and PAV aged binders, respectively.

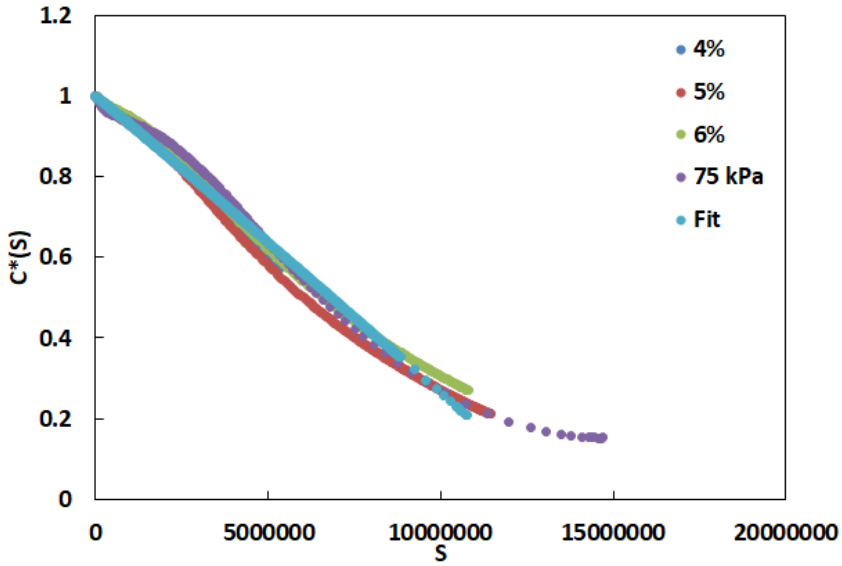

Figure 5.28 Damage characteristic curve for RTFOT aged binder in strain control and stress controled time sweep tests

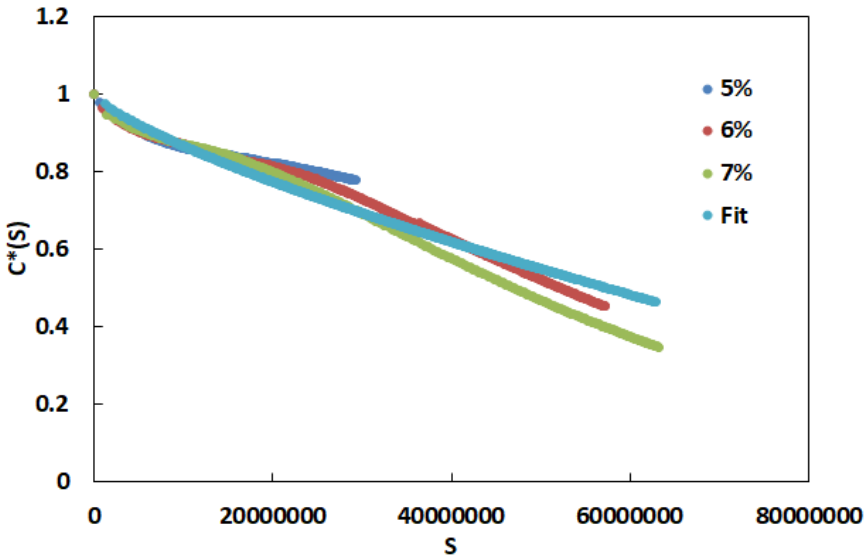

Figure 5.29 Damage characteristic curve for PAV aged binder in strain controlled time sweep tests

The damage characteristic curves for the sand asphalt mixture samples and the fit of Equation (5.10) are shown in Figure 5.30, Figure 5.31, and Figure 5.32, which represent the unaged, RTFOT aged, and PAV aged sand asphalt mixture samples, respectively.

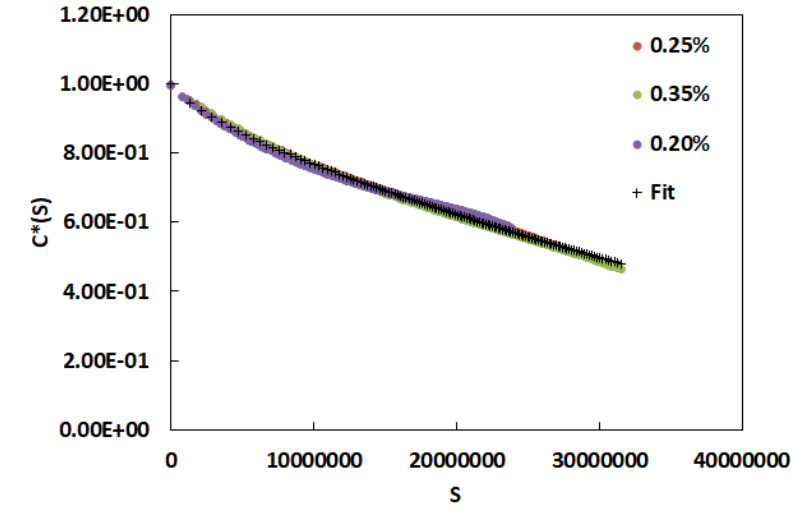

.

Figure 5.30 Damage characteristic curve for unaged sand asphalt

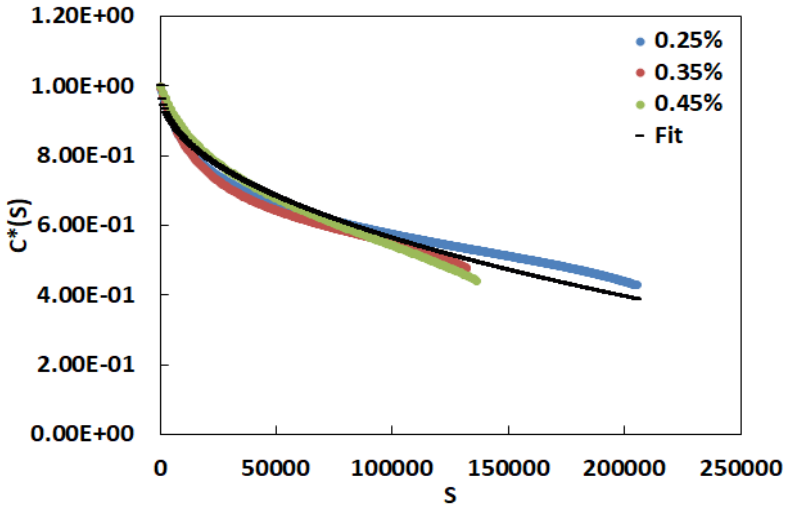

Figure 5.31 Damage characteristic curve for RTFOT aged sand apshalt

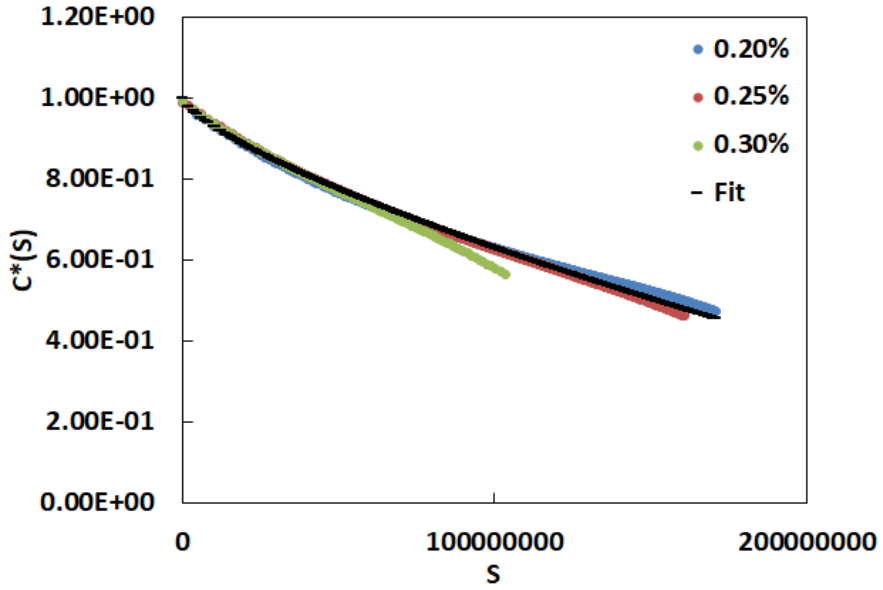

Figure 5.32 Damage characteristic curve for PAV aged sand aspahlt sample

Important to the fatigue analysis is the failure criterion to define fatigue failure of the sample. In this study, as mentioned earlier, the G^R based criterion was used to characterize damage evolution in both binder and sand asphalt mixture samples. The average released pseudo strain energy versus the failure correlated well across different testing conditions, as observed in Figure 5.33 and Figure 5.34. In this way, one can unify different testing methods such as the time sweep stress controlled, time sweep strain controlled, LAS-1, and LAS-2, and the effect of testing temperature. Safaei et al. [19] incorporated the G^R to develop a fatigue characterization method, as described below. The released pseudo strain energy in a given cyclic load can be calculated as:

$$W_r^R = \frac{1}{2}(1 - C^*)\left(\gamma_p^R\right)^2 \tag{5.13}$$

$$G^R = \frac{\overline{W_r^R}}{N_f} = \frac{A}{N_f^2} \tag{5.14}$$

where $\overline{W_r^R}$ is the average released pseudo strain energy until failure, defined as:

$$\overline{W_r^R} = \frac{A}{N_f} \tag{5.15}$$

where *A* is the total released pseudo strain energy until failure in the fatigue tests.

G^R and the number of cycles to failure are related using a simple power law as follows:

$$G^R = \mathrm{a}\left(N_f\right)^b \tag{5.16}$$

To demonstrated how it works, the fit using Equation (5.16) is exemplified in Figure 5.33 and Figure 5.34 for the unaged binder and the RTFOT aged sand asphalt mixture. The figures show the unifying approach adopted by using the average pseudo strain energy released during the different fatigue tests. The parameters obtained by fitting Equations (5.10) and (5.16) are presented in Table 5.3.

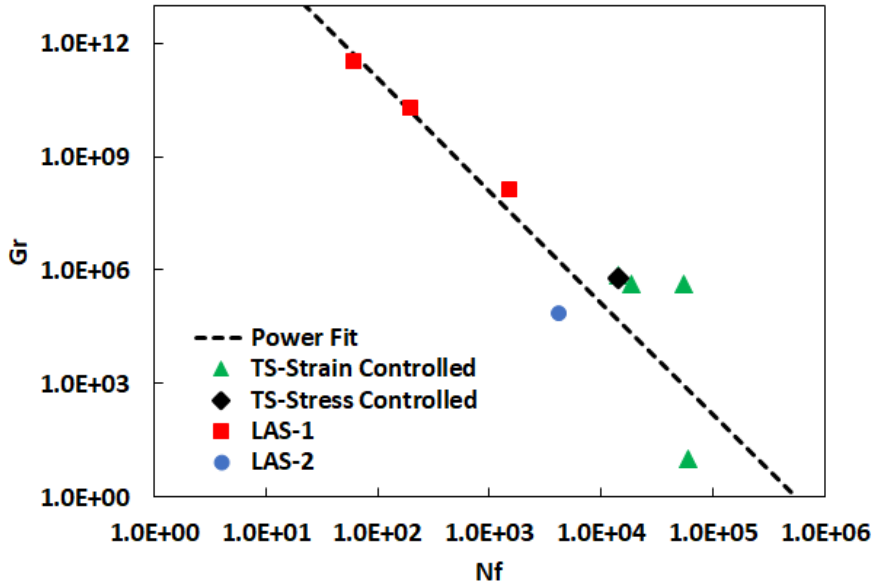

Figure 5.33 G^R vs N_f for unaged binder obtained time sweep and LAS tests

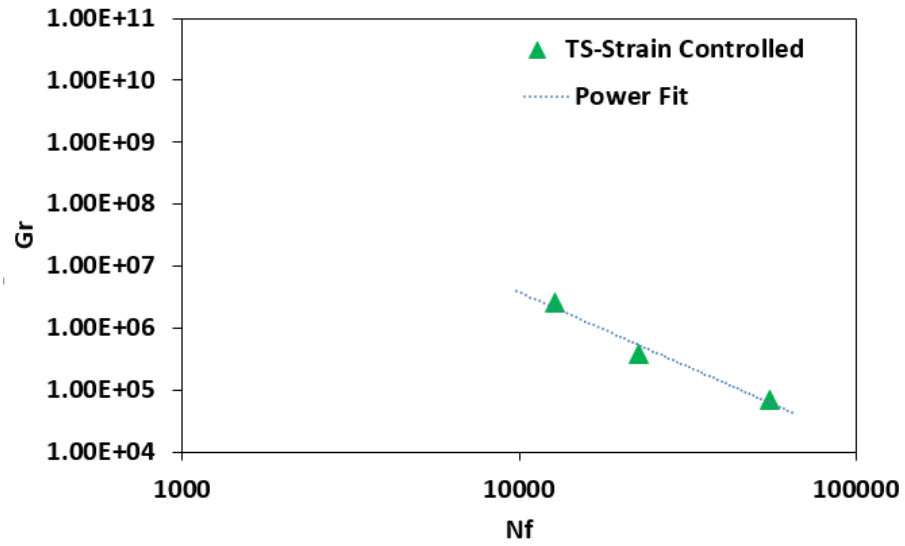

Figure 5.34 G^R vs N_f for RTFOT aged sand asphalt obtained using time sweep tests

The resulting fatigue life for the binder and sand asphalt mixture at different aging levels are shown in Figure 5.35 and Figure 5.36, respectively. Figure 5.35 shows that fatigue resistance of unaged binder is less than PAV aged case, which

contrasts to the common belief that aging would accelerate fatigue damage in pavements. On the other hand, in the case of sand asphalt sample, the fatigue lives of the unaged and RTFOT aged sand asphalt mixture were relatively similar at the strain levels tested in this study and they were longer than the PAV aged samples.

Table 5.3 Fit parameters for damage characteristic curve and G^R vs N_f

	Aging	α	C_1	C_2	a	b
Binder	Unaged	1.2	3.31E-05	0.6383	1.00E+17	-2.962
	RTFOT aged	1.3	5.45E-08	1.0186	7.00E+15	-2.257
	PAV aged	1.5	7.51E-07	0.7506	3.00E+16	-1.951
Sand Asphalt Mixture	Unaged	2.2	2.75E-06	0.7038	1.00E+10	-1.212
	RTFOT aged	0.37	2.00E-03	0.4677	2.00E+16	-2.402
	PAV aged	3	5.93E-07	0.7244	2.00E+08	-0.688

Results from the sand asphalt testing were closer to the general belief/observations than the DSR binder testing, which might be due to the fact that binder phase existing in a very thin film in sand asphalt mixture is more realistic and representative than the 2-mm thick binder used for binder fatigue testing. Figure 5.37 shows the predicted and the experimental values for binder and sand asphalt mixture samples. It shows good predictions for unaged binder and sand aasphalt mixture. PAV aged sand asphalt mixture sample was excluded due to poor correlations.

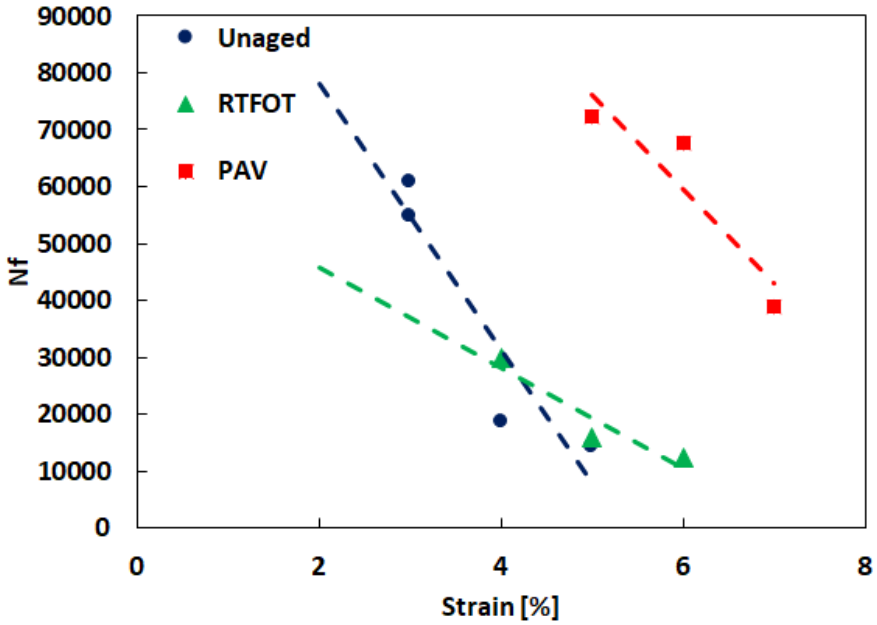

Figure 5.35 Fatigue life for binder across different aging conditions

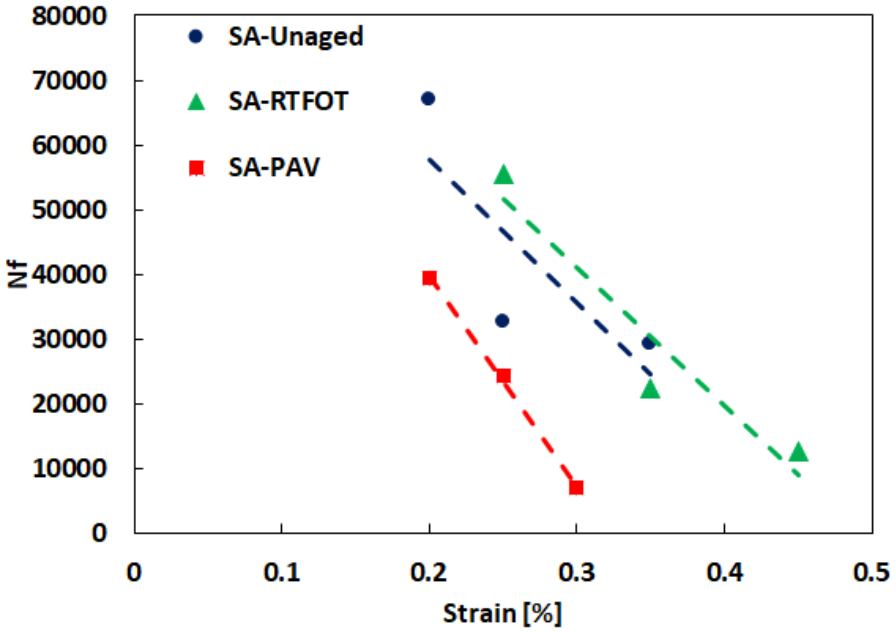

Figure 5.36 Fatgue life for sand asphalt mixture across different aging conditions

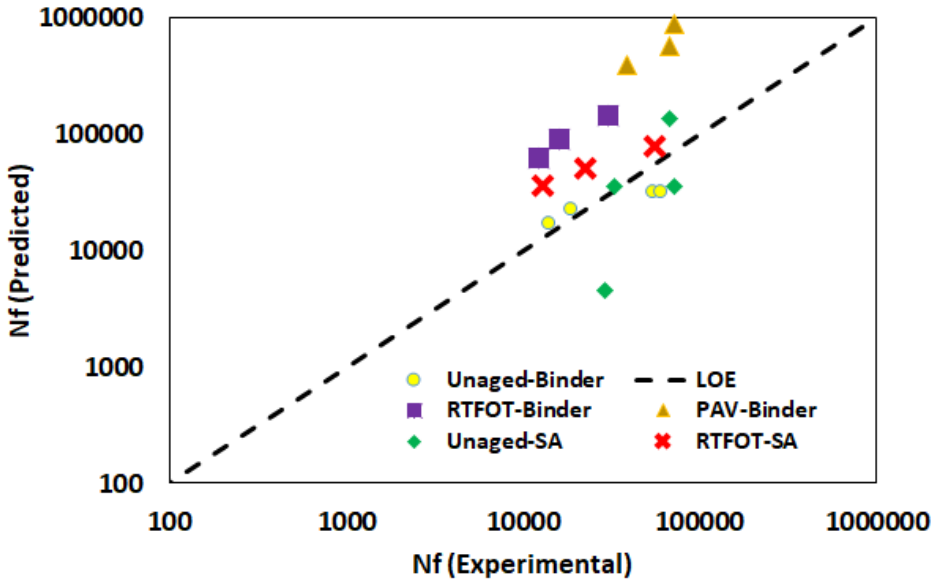

Figure 5.37 Fatigue life predicted vs experimental values for binder and sand asphalt mixture samples under different aging conditions

CHAPTER SIX

CONCLUSION

6.1 Findings

This study presents a linear viscoelastic analysis and fatigue damage characterization at two different length scales: the binder level and the sand asphalt mixture level. This study investigated the influence of a thin film of binder on the linear viscoelastic behavior and fatigue damage resistance. The effect of different modes of loading, either in strain controlled or stress controlled mode of loading, was investigated under the influence of aging. Based on the test results and relevant analyses, the following conclusions can be drawn.

1. The binder strongly influenced the linear viscoelastic properties of the sand asphalt mixture. The sand mixture was modeled as a viscoelastic solid-like material, while binder was modeled as a viscoelastic fluid-like material.
2. From the binder fatigue tests, particularly for the strain controlled time sweep testing mode, there was no clear peak in C* x N for unaged and the RTFOT aged binder in evaluating the fatigue failure point. Stress controlled fatigue tests showed clearer distinction in this regard. In the case of the sand asphalt samples, this was not an issue. Irrespective of the mode of loading, indicators such as points of inflection in the $|G^*|$ vs N, peak in the phase angle, and C^* x N were clearly seen to be used simultaneously to evaluate progressive fatigue damage.
3. Strain controlled time sweep tests of sand asphalt mixtures showed similar behavior from the stress controlled time sweep fatigue tests of binders.
4. From the time sweep fatigue tests of unaged and RTFOT aged sand asphalt samples, two inflection points were noticed in the phase angle. After the first

point of inflection, a steady growth in the phase angle was observed, indicating the manifestation of small cracks that later coalesce to larger cracks after the second inflection point.

5. From the strain controlled mode binder fatigue tests at 25 °C, considerable edge effects were observed during the test. A plateau region appeared in the phase angle is an indication of the onset of the edge effects or plastic flow. This was usually seen from unaged and RTFOT aged binders. Such effects could be reduced by performing the tests at relatively lower temperatures (such as below 20 °C). This was not observed in the case of the PAV aged samples.
6. It was observed that G^R based energy dissipation criterion for the binder evaluated a reasonable estimate for fatigue damage at relatively lower temperatures, but was limited to capture the influence of aging.
7. Sand asphalt mixture testing could capture the microcracking and macrocracking phases more distinctively when compared to binder testing. In the case of pressure aging vessel (PAV) aged samples, it was observed that the macrocracking phase disappeared and was replaced by sudden changes in the material properties, indicating that the PAV aged mixture was more susceptible to fatigue cracking.
8. By incorporating test results with the simplified viscoelastic continuum damage approach, it was found that the sand asphalt mixture testing was better to capture the influence of aging and changes in the microstructure during fatigue process in comparison to binder fatigue tests using 2-mm thick disc.

6.2 Future Work

1. The binder film thickness in the sand asphalt mixture samples plays a prominent role in the fatigue behavior of the mixture. Hence, further studies investigating the influence of different film thickness on the fatigue resistance are recommended
2. Moreover, the film thickness should be representative of what one can expect for a given AC mix design. Hence, a standardized sample preparation methodology of the sand mixture or so needs to be developed.
3. Linear amplitude sweep is a much faster test methodology when compared to time sweep fatigue tests. The G^R based failure criterion could unify the two test methods for the binder, but was somewhat limited to the sand asphalt mixture samples. Hence, an improved method that can unify different test conditions for sand mixtures is necessary.
4. In the fatigue tests performed on the binder and the sand asphalt mixture samples herein, the strain/stress applied were large enough to be well within a much more complicated material behavior including linear viscoelastic, nonlinear viscoelastic as well as fatigue damage. The nonlinear viscoelastic behavior and its contribution was not considered in this study. Thus, it would be recommended to characterize the test results by considering more relevant material responses to more accurately understand the complex behavior.

References

1. Branco, V.T.F.C. A unified method for the analysis of nonlinear viscoelasticity and fatigue cracking of asphalt mixtures using the dynamic mechanical analyzer [dissertation]. Texas A&M University; 2008.

2. Di Benedetto H, Olard F, Sauzat C, Delaporte B. Linear viscoelastic behaviour of bituminous materials: From binders to mixes. Road Materials and Pavement Design. 2004;5(sup1):163-202.

3. Wang C, Castorena C, Zhang J, Richard Kim Y. Unified failure criterion for asphalt binder under cyclic fatigue loading. Road Materials and Pavement Design. 2015;16(sup2):125-48.

4. Masad E, Somadevan N. Microstructural finite-element analysis of influence of localized strain distribution on asphalt mix properties. J Eng Mech. 2002;128(10):1105-14.

5. Drakos C, Roque R, Birgisson B. Effects of measured tire contact stresses on near-surface rutting. Transportation Research Record: Journal of the Transportation Research Board. 2001(1764):59-69.

6. Lakes RS, Kose S, Bahia H. Analysis of high volume fraction irregular particulate damping composites. Journal of engineering materials and technology. 2002;124(2):174-8.

7. Kose S. Development of a virtual test procedure for asphalt concrete [dissertation]. University of Wisconsin--Madison; 2002.

8. Hajj R, Bhasin A. The search for a measure of fatigue cracking in asphalt binders–a review of different approaches. International Journal of Pavement Engineering. 2017:1-15.

9. Tsai B, Monismith CL, Dunning M, Gibson N, D'Angelo J, Leahy R, et al. Influence of asphalt binder properties on the fatigue performance of asphalt concrete pavements. Journal of the Association of Asphalt Paving Technologists. 2005;74:733-89.

10. Bahia HU, Zhai H, Bonnetti K, Kose S. Non-linear viscoelastic and fatigue properties of asphalt binders. Journal of the Association of Asphalt Paving Technologists. 1999;68:1-34.

11. Bahia HU, Hanson DI, Zeng M, Zhai H, Khatri MA, Anderson RM. Characterization of modified asphalt binders in superpave mix design. ; 2001.

12. Anderson D, Hir Y, Marasteanu M, Planche J, Martin D, Gauthier G. Evaluation of fatigue criteria for asphalt binders. Transportation Research Record: Journal of the Transportation Research Board. 2001(1766):48-56.

13. Kim Y, Little DN, Lytton RL. Use of dynamic mechanical analysis (DMA) to evaluate the fatigue and healing potential of asphalt binders in sand asphalt mixtures (with discussion and closure). Journal of the Association of Asphalt Paving Technologists. 2002;71.

14. Martono W, Bahia HU, D'angelo J. Effect of testing geometry on measuring fatigue of asphalt binders and mastics. J Mater Civ Eng. 2007;19(9):746-52.

15. Underwood BS, Kim YR, Guddati MN. Improved calculation method of damage parameter in viscoelastic continuum damage model. International Journal of Pavement Engineering. 2010;11(6):459-76.

16. Schapery RA. Correspondence principles and a generalizedJ integral for large deformation and fracture analysis of viscoelastic media. Int J Fract. 1984;25(3):195-223.

17. Kim Y, Little DN. Linear viscoelastic analysis of asphalt mastics. J Mater Civ Eng. 2004;16(2):122-32.

18. Park SW, Schapery RA. Methods of interconversion between linear viscoelastic material functions. Part I—A numerical method based on Prony series. Int J Solids Structures. 1999;36(11):1653-75.

19. Safaei F, Castorena C, Kim YR. Linking asphalt binder fatigue to asphalt mixture fatigue performance using viscoelastic continuum damage modeling. Mechanics of Time-Dependent Materials. 2016;20(3):299-323.

20. Rowe GM, Bouldin MG. Improved techniques to evaluate the fatigue resistance of asphaltic mixtures. 2nd Eurasphalt & Eurobitume Congress Barcelona; ; 2000.

21. Wang C, Zhang H, Castorena C, Zhang J, Kim YR. Identifying fatigue failure in asphalt binder time sweep tests. Constr Build Mater. 2016;121:535-46.

22. Sabouri M, Kim Y. Development of a failure criterion for asphalt mixtures under different modes of fatigue loading. Transportation Research Record: Journal of the Transportation Research Board. 2014(2447):117-25.

23. Wang C, Castorena C, Zhang J, Richard Kim Y. Unified failure criterion for asphalt binder under cyclic fatigue loading. Road Materials and Pavement Design. 2015;16(sup2):125-48.